AGU PUBLICATIONS

Water Resources Research

RESEARCH ARTICLE
10.1002/2015WR017244

Key Points:
- Stomatal conductance is modeled using physical equations with xylem cavitation
- Simulation of drought transpiration and leaf water potential was improved
- Transient response to cavitation helps to explain optimal hydraulic traits

Supporting Information:
- Supporting Information S1

Correspondence to:
D. S. Mackay,
dsmackay@buffalo.edu

Citation:
Mackay, D. S., D. E. Roberts, B. E. Ewers, J. S. Sperry, N. G. McDowell, and W. T. Pockman (2015), Interdependence of chronic hydraulic dysfunction and canopy processes can improve integrated models of tree response to drought, *Water Resour. Res.*, *51*, 6156–6176, doi:10.1002/2015WR017244.

Received 16 MAR 2015
Accepted 10 JUL 2015
Accepted article online 14 JUL 2015
Published online 6 AUG 2015

Interdependence of chronic hydraulic dysfunction and canopy processes can improve integrated models of tree response to drought

D. Scott Mackay[1], David E. Roberts[1,2], Brent E. Ewers[3], John S. Sperry[4], Nathan G. McDowell[5], and William T. Pockman[6]

[1]Department of Geography, University at Buffalo, Buffalo, New York, USA, [2]Now at Resource Data Inc., Portland, Oregon, USA, [3]Department of Botany and Program in Ecology, University of Wyoming, Laramie, Wyoming, USA, [4]Department of Biology, University of Utah, Salt Lake City, Utah, USA, [5]Earth and Environmental Sciences Division, Los Alamos National Laboratory, Los Alamos New Mexico, USA, [6]Biology Department, University of New Mexico, Albuquerque, New Mexico, USA

Abstract Hydraulic systems of plants have evolved in the context of carbon allocation and fitness trade-offs of maximizing carbon gain and water transport in the face of short and long-term fluctuations in environmental conditions. The resulting diversity of traits include a continuum of isohydry-anisohydry or high to low relative stomatal closure during drought, shedding of canopy foliage or disconnecting roots from soil to survive drought, and adjusting root areas to efficiently manage canopy water costs associated with photosynthesis. These traits are examined within TREES, an integrated model that explicitly couples photosynthesis and carbon allocation to soil-plant hydraulics and canopy processes. Key advances of the model are its ability to account for differences in soil and xylem cavitation, transience of hydraulic impairment associated with delayed or no refilling of xylem, and carbon allocation to plant structures based on photosynthetic uptake of carbon and hydraulic limitations to water transport. The model was used to examine hydraulic traits of cooccurring isohydric (piñon pine) and anisohydric (one-seed juniper) trees from a field-based experimental drought. Model predictions of both transpiration and leaf water potential were improved when there was no refilling of xylem over simulations where xylem was able refill in response to soil water recharge. Model experiments with alternative root-to-leaf area ratios ($R_{R/L}$) showed the $R_{R/L}$ that supports maximum cumulative water use is not beneficial for supporting maximum carbon gain during extended drought, illustrating how a process model reveals trade-offs in plant traits.

1. Introduction

Plant transpiration is hydrologically important because globally it returns an average of 40 percent of annual precipitation back to the atmosphere [*Berry et al*., 2010; *Fisher et al*., 2011] representing between 35 and 100 percent of total evapotranspiration [*Schlaepfer et al*., 2014]. It is biologically important because plants transpire up to 1000 molar units of water to acquire one molar unit of CO_2 via photosynthesis [*Larcher*, 2003]. Consequently, plants have evolved efficient hydraulic systems capable of transpiring large quantities of water. It is notable that because plant hydraulic systems evolved primarily to support carbon uptake, models of plant hydraulics without carbon metabolism will not give us predictive understanding of system changes such as those due to climate fluctuations and land cover change. These models may get the right answers for the wrong reasons.

Plant hydraulic systems are comprised of the hydraulic properties of the soil, rhizosphere-root flux capacity, dynamic hydraulic conductance due to cavitation of plant xylem, properties of cell membranes, and stomatal conductance. Plants are vulnerable to cavitation [*Tyree and Sperry*, 1989] because water moving within the xylem under tension promotes air seeding across pit membranes, induces a phase change from liquid to gas, and forms embolisms [*Pockman et al*., 1995], which impairs water transport. With reduced transport capacity, at least instantaneously, a smaller amount of xylem is supplying the entire canopy and so leaf water potential, Ψ_L, is decreased if the canopy does not respond by reducing canopy average stomatal conductance, G_L. If G_L remains high, the decrease in water potential in active pathways of the supply system

can initiate a feedback that increases the rate of embolism formation [*Franks*, 2004; *Holtta et al*., 2009; *Meinzer et al*., 2009; *Tyree and Sperry*, 1988]. When plants reduce stomatal conductance during periods of water shortage, they offset this positive feedback by limiting the increase in tension. A consequence is that at short timescales stomata appear to manage an economic trade-off between carbon gain and water loss [*Katul et al*., 2009]. At long timescales (e.g., days to years) plants appear to optimally allocate carbon and energy to structures, e.g., fine roots and leaves, to minimize water and other resource limitations [*Johnson et al*., 2013] and to maximize carbon uptake [*Nolf et al*., 2013]. Classic studies showed strong relationships between total leaf biomass and available soil water spanning shrub to forest ecosystems [*Grier and Running*, 1977; *Gholz*, 1982]. Theory and data suggest that reduced leaf area associated with chronically low soil moisture is coordinated with other morphological changes such as increased root areas and root depths [*Hacke et al*., 2000; *Magnani et al*., 2002]. These trade-offs are important because water demand in excess of available water supply has been, and continues to be, a focus of simulation models of plants.

As Ψ_S declines plants close stomata either directly or in concert with chemical signals [*Comstock*, 2002] in response to hydraulic signals [*Blackman et al*., 2009; *Brodribb and McAdam*, 2013; *Franks et al*., 2007; *McAdam and Brodribb*, 2014]. This occurs along a continuum of isohydric and anisohydric responses [*Klein*, 2014; *Tardieu and Simonneau*, 1998]. Isohydric plants reduce canopy average stomatal conductance, G_L, to prevent minimum Ψ_L, which occurs at peak transpiration, from declining with Ψ_S. Anisohydric plants keep G_L relatively higher and thus allow minimum Ψ_L to decline with Ψ_S as long as Ψ_L remains above a critical threshold [*Kolb and Sperry*, 1999]. The isohydry-anisohydry continuum can be informative when making comparisons among plant hydraulic traits within a particular climate-soil regime because a relatively anisohydric plant may be able to continue to extract water at low Ψ_S when isohydric species have closed their stomata [*Sperry and Hacke*, 2002].

Once emboli have formed, flow continues through adjacent functional xylem conduits, bypassing embolized conduits at the cost of reduced overall hydraulic conductance, *K*. Refilling, if it can occur, requires carbon and energy, which may be in short supply especially for isohydric plants [*Dickman et al*., 2014] if stomata have been closed for an extended period [*Mitchell et al*., 2013]. Alternatively, anisohydric plants continue to acquire carbon during drought, but may be at risk of hydraulic failure if their stomata remain open too long under low Ψ_S conditions [*Brodribb and Cochard*, 2009; *McDowell et al*., 2008]. Embolism repair or new xylem growth may not occur at critical points in time to avert carbon deficiency or hydraulic failure because xylem refilling after drought stress is relieved is not universal [*Cochard and Delzon*, 2013; *Zwieniecki and Holbrook*, 2009]. It is evident that drought can result in chronic hydraulic impairment that lasts months to years [*Anderegg et al*., 2012; *Ewers et al*., 2007; *Hacke et al*., 2001; *Sala et al*., 2010] and for some xylem morphology a progressive increase in vulnerability to cavitation, which is sometimes referred to as cavitation fatigue [*Anderegg et al*., 2012; *Hacke et al*., 2001]. Some physiological and structural responses to chronic hydraulic dysfunction may prolong survival during drought. One drought-related structural change, leaf abscission, appears to be a water saving strategy often associated with anisohydry [*Maseda and Fernandez*, 2006], but also seen with isohydric species [*Bucci et al*., 2005], while hydraulic isolation of roots to reduce water loss to the soil is associated with isohydric species [*Limousin et al*., 2009; *Maseda and Fernandez*, 2006; *Plaut et al*., 2013]. Such structural changes also impede recovery when drought is relieved. Consequently, whole plant physiology can set up long lags between soil water recovery from drought and plant responses to the recovery. But models predict, as some but not all field data show, an immediate response of the plant when drought in the soil is relieved.

In contrast to the lack of universal xylem refilling seen with whole plant physiology, process models assume that xylem hydraulic conductance fully recovers as soon as drought in the soil is relieved. This large gap between physiology and process models is not addressed just by introducing plant hydraulics into the models. Even models that have profited from the use of plant hydraulics assume immediate recovery of xylem conductance as Ψ_S increases [*Bohrer et al*., 2005; *Da Silva et al*., 2011; *Domec et al*., 2012; *Hickler et al*., 2006; *Holtta et al*., 2006, 2009; *Janott et al*., 2010; *Magnani et al*., 2002; *Quijano et al*., 2012; *Tuzet et al*., 2003; *Williams et al*., 1996, 2001]. A notable exception is *Manzoni et al*. [2014] who allowed for an empirical down regulation of drought recovery. The prevailing assumption in models may be justified in terms of long-term adaptation of vulnerability to cavitation, or acclimation of leaf area and root architecture to average soil moisture dynamics. But long-term averages are not of much help for predicting realistic growth rates when climate is changing or when there are new disturbances. Consequently, a necessary control over both canopy gas exchange and adjustments to root and leaf area, is the time lag between the onset of cavitation and when refilling of xylem occurs at seasonal to interannual timescales. In the absence of refilling of xylem,

a decoupling can develop between soil and plant water status, particularly for plants exposed to frequent drought cycles or prolonged periods of severe drought.

To address the gap between empirical data and existing models, we sought to develop an integrated model that computes G_L in terms of photosynthesis, soil-plant hydraulics, and chronic hydraulic impairment. The model is used to explore how these integrative controls affect root water uptake and allocation of carbon to leaf area during drought. The model is then used to gain insights on potentially optimal root architectures and root-leaf area proportionality. Specifically we asked: Does chronic hydraulic impairment impact optimal root area or its distribution with depth? Can it explain differential hydraulic failure of roots and canopy during drought? We begin by developing the conceptual basis for the model, describe the key integrated model components, and evaluate the model in simulating the response of relatively isohydric and anisohydric trees to a multiyear experimental drought [*McDowell et al*., 2013]. The current study improves on the previously described Terrestrial Regional Ecosystem Exchange Simulator (TREES) [*Loranty et al*., 2010a,b; *Mackay et al*., 2012; *McDowell et al*., 2013] model by tightly coupling the stomatal conductance to the transpiration-tension function, more formally defining memory of hydraulic impairment, and adding feedback between hydraulics and carbon allocation to leaves and roots.

2. Methods

2.1. Conceptual Framework

Canopy gas exchange manages a trade-off between carbon uptake and the instantaneous demand-supply of water. The supply of water for transpiration per unit leaf area (E_L) (mmol m^{-2} s^{-1}) can be expressed as a function of the variability in soil-plant hydraulic conductance per unit leaf area [$(K(\Psi)_L)$] (mmol m^{-2} s^{-1} MPa^{-1}) with the tension gradient along the path from soil-to-leaf [after *Whitehead and Jarvis*, 1981] as:

$$E_L = K(\Psi)_L \cdot (\Psi_S - \Psi_L - \rho g h) \tag{1}$$

where Ψ_S and Ψ_L are soil and leaf water potentials (MPa), respectively, h is height, ρ is density of water, and g is acceleration due to gravity.

Canopy water demand can be expressed conceptually with Fick's Law of diffusion as

$$E_L = G_{LV} \cdot [e_S(T_L) - e_a] \cong G_{LV} D_M \tag{2}$$

where G_{LV} is canopy average stomatal conductance per unit leaf area (mmol m^{-2} s^{-1}) for water vapor, $e_s(T_L)$ is the molar concentration vapor pressure of the air in contact with the evaporating water surface in the stomatal cavity, e_a is the molar concentration vapor pressure of the air at the leaf surface, and D_M is vapor pressure deficit in molar concentration units. By substituting equation (1) into equation (2), G_{LV} can be expressed in terms of both water supply and demand assuming no capacitance:

$$G_{LV} = K(\Psi)_L \cdot (\Psi_S - \Psi_L - \rho g h) \cdot D_M^{-1}. \tag{3}$$

The relative importance of the role of gravitational potential compared to path-length resistance [*Hubbard et al*., 1999; *Schafer et al*., 2000] is yet unknown [*Domec et al*., 2008]. Regardless, for plants shorter than 10 m gravitational potential is relatively small (i.e., 0.098 MPa for each 10 m increase in height). In general, if $h \ll \frac{\Psi_S - \Psi_L}{\rho g}$, then

$$G_{LV} = K(\Psi)_L \cdot (\Psi_S - \Psi_L) \cdot D_M^{-1}. \tag{4}$$

Equation (4) describes stomatal conductance in terms of soil-plant hydraulic limits and atmospheric demand for water, but other factors such as light and temperature should also be accounted for. These other factors can be expressed through their role on photosynthesis, by recognizing that stomata open for carbon uptake while also keeping the water demand minus supply within hydraulically safe limits. Canopy average stomatal conductance per unit leaf area for carbon, G_{LC}, can be expressed as

$$G_{LC} = \frac{A_L}{c_a - c_i} \tag{5}$$

where A_L is photosynthetic carbon assimilated per unit leaf area (μmol m^{-2} s^{-1}), and c_a and c_i are molar fractions of CO_2 in leaf surface and intercellular air masses, respectively. Assuming $G_{LV} = aG_{LC}$ and no other

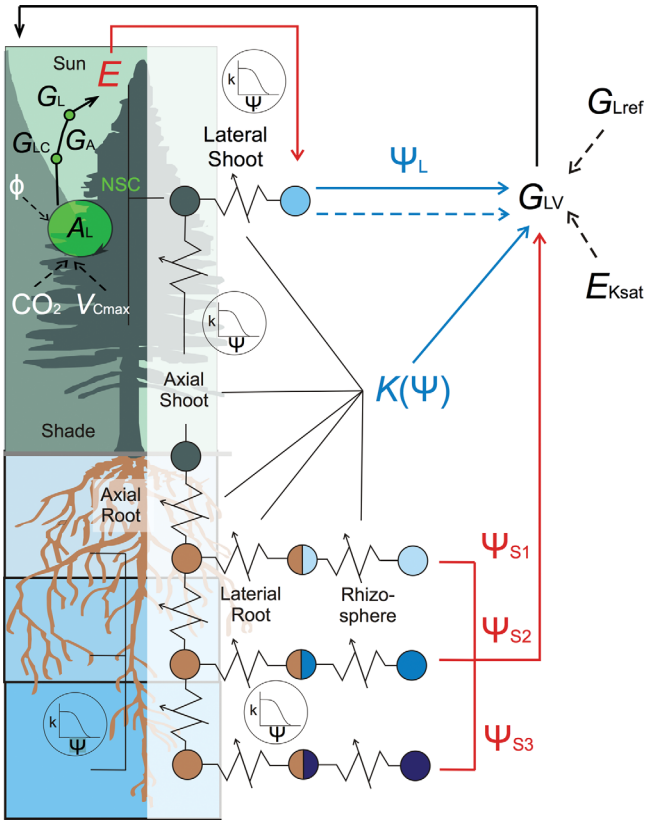

Figure 1. Conceptual diagram for the Terrestrial Regional Ecosystem Exchange Simulator (TREES) showing three root modules and one shoot module with sun and shade elements. Each root module is connected to its respective rhizosphere and bulk soil. The primary solution is for canopy average stomatal conductance (G_L). Vulnerability (K-Ψ) curves are assigned to lateral shoot/branch, axial shoot, axial root, and lateral root. Red lines denote boundary conditions, transpiration (E), and soil water potentials (Ψ_S). Blue lines show hydraulic conductivity [$K(\Psi)$], leaf water potential (Ψ_L), and critical transpiration rate (E_{Crit}). Parameter inputs are stomatal conductance at vapor pressure deficit of 1 kPa (G_{Sref}) and transpiration at saturated hydraulic conductivity (E_{Ksat}). Photosynthesis (A_L) and its main inputs (maximum carboxylation (V_{Cmax}), quantum yield (ϕ), and CO_2), stomatal conductance of carbon (G_{LC}), aerodynamic conductance (G_A), and nonstructural carbon (NSC) are also depicted.

conductances besides stomatal, where $a = 1/1.6$ is a molar conversion constant between water vapor and CO_2 conductance, then equations (4) and (5) are combined to express the hydraulic requirements for balancing photosynthetic carbon uptake and water loss:

$$K(\Psi, A_L)_L = \frac{D_M}{\Psi_S - \Psi_L} \cdot \frac{a \cdot A_L}{c_a - c_i}. \quad (6)$$

We implemented this coupled water and carbon flow in TREES, using equation (4) for the whole-plant and equation (5) for sun and shade canopy elements. The $K(\Psi)$ and $K(A_L)$ terms in equation (6) require models in and of themselves. In particular, $K(\Psi)$ is a complex function because Ψ varies along the continuum, the vulnerability to cavitation varies along the continuum, and the rhizosphere vulnerability is usually different from the xylem vulnerability. Consequently, to compute rhizosphere [*Campbell*, 1985] and plant hydraulics, including K_L and Ψ_L, we integrated the soil-plant water transport model [*Sperry et al.*, 1998] into TREES (Figure 1). The combined model is implemented in C++ compiler.

2.2. Computation of Stomatal Conductance

To solve equation (6), we needed to compute Ψ_L, which the plant water transport model predicts for given a value of E_L. To solve for E_L, we in turn need G_{LV}, and so we started with an initial guess at G_{LV}, from which we computed an initial E_L, predicted Ψ_L, and then recomputed G_{LV} using equation (4). The algorithm followed five steps in an iterative solution. At step (1), an initial guess of G_{LV} (G_{LV0}) was computed using

$$G_{LV0} = w_s(G_{Lref} - m \ln D), \quad (7)$$

where w_s is an integral measure of soil and plant water stress that is nonlinearly related to tension (see below), G_{Lref} is reference canopy average stomatal conductance at $D = 1$ kPa, and m is the gain of the stomatal conductance response to a change in D [*Oren et al.*, 1999]. We set $m = 0.54\ G_{Lref}$ based on a theoretical relationship that holds across many species [*Katul et al.*, 2009] and used G_{Lref} as a measurable parameter. We found no evidence of a need for a lower value of m and even experimented with values of m between 0.3 and 0.54. At step (2), G_{LV0} was used to compute sun and shade leaf temperatures [*Campbell and Norman*, 1998]. G_{LV0} and sun and shade temperatures were used as inputs to the Farquhar photosynthesis model [*Farquhar and Sharkey*, 1982; *Farquhar et al.*, 1980] to compute A_L in sun and shade elements [*dePury and Farquhar*, 1997]. In order to allow photosynthesis to influence sun and shade element stomatal conductance and in turn transpiration, we also computed c_i in both sun and shade elements using the steady state model derived by *Katul et al.* [2003], and then G_{LC} in sun and shade elements using equation (5). The details on

how these computations are implemented in TREES were previously described [*Loranty et al.*, 2010b]. Both the Farquhar and Katul models need maximum carboxylation rate, V_{cmax} (μmol m^{-2} s^{-1}), and quantum yield, φ (mol CO_2 mol photons^{-1}) [*Singsaas et al.*, 2001], and these were derived from leaf gas exchange [*Mackay et al.*, 2012]. At step (3), for both sun and shade elements, canopy conductance, G_L, was computed from G_{LC} and aerodynamic conductance, G_A [*Samanta et al.*, 2007], and then G_L was used to compute sun and shade transpiration using the Penman-Monteith equation [*Mackay et al.*, 2012]. Whole-canopy E_L was computed by summing the transpiration values, weighting them by their respective sun and shade leaf area. At step (4), K_L and Ψ_L were computed by solving the soil-leaf hydraulic continuum with E_L as the boundary condition on one end of the continuum and bulk soil water in each layer as other boundary conditions. The details on this solution are provided in section 2.3. At step (5), K_L and Ψ_L were used to recompute G_{LV} using equation (4). The algorithm iterated over steps (2–5) using G_{LV} instead of G_{LV0} until the difference in E_L between iterations converged on zero.

We used equation (7) as the initial guess G_{LV0}, as it generally minimized the number of iterations needed for the algorithm to converge when used in conjunction with a known w_s computed from the previous time step. A number of plant hydraulic properties were explored to define w_s, e.g., K_L relative to K_{sat} (saturated hydraulic conductivity), Ψ_L relative to Ψ_{Crit} (critical or minimum tension), and E_{Lcrit} (maximum safe or critical transpiration) relative to E_L at K_{sat}. E_{Lcrit} proved to be a robust measure of soil-plant water status as it declined slowly and monotonically between soil rewetting events. Consequently, w_s at time step t was computed as the ratio of E_{Lcrit} at $t-1$ to unstressed E_L at K_{sat}, which was parameterized from sap flux data on a day when soil water was not limiting [*McDowell et al.*, 2013]. Corresponding unstressed predawn and midday Ψ_L values were obtained for the same day. G_{Lref} was estimated using boundary line analysis of sap flux and micrometeorological data [*Ewers et al.*, 2007], which provides a robust estimate of maximum, unstressed G_{Lref}. All other input parameters were either derived from previous studies or obtained from site-specific measurements (see Table 1). TREES is sensitive to root-to-leaf area ratio, soil texture, and vulnerability to cavitation parameters, in particular, and these sensitivities are explored with the simulation experiments described below.

2.3. Computation of Soil and Plant Water Dynamics

Water balance was simulated using a quasisteady solution of the soil-plant hydraulic continuum at 30 min time steps. The plant root profile depth was divided into soil-root layers (three in the present study) each comprised of bulk soil, rhizosphere, lateral root, and axial root elements. A litter layer with no roots capped the shallowest layer. The change in water content in each soil-root layer was computed by (1) adding excess water from the litter layer during precipitation events to the shallowest soil-root layer, (2) moving water to successive soil-root layers using an explicit, iterative solution of the Richards equation with a van Genuchten soil water retention parameterization [*Van Genuchten*, 1980], and (3) adding or subtracting fluxes of water between the roots and bulk soil via the rhizosphere. There were no horizontal transfers of water into and out of the system, and the base of the lowest soil-root layer had a free-drainage boundary condition. Evaporation from the litter layer or a linear mix of bare soil and litter where there is partial litter cover, followed Penman-Monteith [*Monteith*, 1965].

For brevity we do not go into all the details on rhizosphere and plant water transport [*Sperry et al.*, 1998], but focus on how it is implemented within TREES. The rhizosphere-to-leaf catena was organized as a set of i elements consisting of nested rhizosphere cylinders, absorbing lateral roots, conducting or axial roots, axial shoot, and a single lateral shoot representing the canopy (Figure 1). For each element water flux (mmol m^{-2} leaf s^{-1}) was computed using the Richards equation with the Kirchoff transform [*Ross and Bristow*, 1990],

$$F_i(\Phi_i, \Phi_{i+1}, \Phi_{i-1}) = (\Phi_i - \Phi_{i-1}) - (\Phi_{i+1} - \Phi_i) - \Delta W_i/\Delta t, \tag{8}$$

where Φ_i is matrix flux potential of the i^{th} xylem element, computed by integrating hydraulic conductance using the complement of an incomplete gamma function [*Press et al.*, 1992],

$$\Phi_i = k_S b/c \int_{z(\Psi_i)}^{z(\infty)} e^{-z} z^{(c^{-1}-1)} dz \tag{9}$$

for $z = (-\Psi_i/b)^c$, k_s is saturated hydraulic conductance of a given plant tissue (mmol m^{-2} s^{-1} MPa^{-1}), Ψ_i is tension of ith element (MPa), and b and c are parameters of the Weibull function that closely fits empirical xylem vulnerability to cavitation curves. ΔW is the change in water content at time t computed as

Table 1. Primary Parameter Inputs to TREES by Source and Type, and Units, for Pine and Juniper at the Sevilleta Drought Experiment[a]

Parameter by Source/Type	Units	Pine	Juniper	Optimality
Measured [*Plaut et al.*, 2013]:				
Ψ_{md} at saturated hydraulic conductivity	MPa	−2.59	−2.63	−2.59
Ψ_{pd} at saturated hydraulic conductivity	MPa	−1.06	−1.19	−1.06
E at saturated hydraulic conductivity	mmol m^{-2} s^{-1}	0.60	0.32	0.60
Weibull b parameter, shoot	Negative MPa	3.43	8.70	3.43, 8.70[b]
Weibull b parameter, root	Negative MPa	3.57	8.70	3.57, 8.70
Weibull c parameter, shoot	Unitless	1.65	3.81	1.65, 3.81
Weibull c parameter, root	Unitless	4.07	3.81	4.07, 3.81
Silt fraction	Unitless	0.4	0.4	0.4, 0.44[c]
Clay fraction	Unitless	0.06	0.06	0.06, 0.10
Soil bulk density	Mg m^{-3}	1.27	1.27	1.27
Calculated [*Campbell*, 1985]:				
Geometric standard deviation of soil particle size	mm	8.8	8.8	8.8, 14.55
Geometric mean particle diameter	mm	0.156	0.156	0.156, 0.102
Porosity	m^3 m^{-3}	0.43	0.43	0.43
Allometric [*Plaut et al.*, 2012]:				
Initial leaf area index	m^2 m^{-2}	1.37	1.19	1.37
Specific leaf area	m^2 leaf area kg^{-1} C	8.0	3.5	8.0
Leaf lifespan	Years	7.0	7.0	7.0
Initial sapwood carbon	g C m^{-2} ground area	680	360	680
Initial root carbon	g C m^{-2} ground area	388	171	388
Initial nonstructural carbon (NSC)	g C m^{-2} ground area	83	66	83
Assumed [This study]:				
Root-to-leaf area ratio	m^2 m^{-2}	2	5	0.5, 0.75, 1, 1.5, 2, 3, 4, 5
Axial length, shoot	m	2.80	2.80	2.80
Axial length, shallow root	m	0.05	0.05	0.233, 0.05[d], 0.065[e]
Axial length, middle root	m	0.13	0.13	0.233, 0.13, 0.195
Axial length, deep root	m	0.52	0.52	0.233, 0.52, 0.78
Lateral length, shoot	m	1.40	1.40	1.40
Lateral length, shallow root	m	1.05	1.05	1.05
Lateral length, middle root	m	1.23	1.23	0.875, 1.23
Lateral length, deep root	m	0.53	0.53	0.7, 0.53
Leaf area fraction, shallow root	Unitless	0.35	0.35	0.33, 0.35
Leaf area fraction, middle root	Unitless	0.50	0.50	0.33, 0.5
Leaf area fraction, deep root	Unitless	0.15	0.15	0.33, 0.15
Calibrated [*McDowell et al.*, 2013]:				
Quantum yield	mol C mol^{-1} photons	0.06	0.06	0.06
Maximum carboxylation rate (V_{cmax})	μmol m^{-2} s^{-1}	26	55	26
Reference stomatal conductance (Gsref)	mmol m^{-2} s^{-1}	20	7	20
Literature [*Running and Gower*, 1991]:				
Root respiration coefficient	g kg^{-1} d^{-1} deg C	1.1	1.1	1.1
Sapwood respiration coefficient	g kg^{-1} d^{-1} deg C	0.2	0.2	0.2
Leaf respiration coefficient	g kg^{-1} d^{-1} deg C	0.4	0.4	0.4

[a]Also shown are adjustments made to determine optimality of root architecture for both pine and juniper.
[b]Weibull curve parameters representing isohydric, anisohydric species.
[c]Soil texture observed at the site, finer texture.
[d]Root parameters representing uniform, variable root area with depth.
[e]Axial root length summing up to 105 cm total root depth.

$$\Delta W_i = f_i \Delta \Psi_i L_T C \tag{10}$$

where f_i is the fraction of the total plant volume in which element i exchanges water, C is whole-plant change in water content per unit change in tension per unit leaf area, which is set to zero for steady state solutions, and L_T is total leaf area. Transient flow was solved by iteratively adjusting Ψ_i until $\sum_{i=1}^{i=n} |F_i|$ converged on zero. Equation (9) allowed each element of the simulated plant to be conceptually equivalent to a measurable part of a real plant, allowing for input of measured vulnerability to cavitation curves for lateral and axial roots and axial and lateral stems.

The boundary conditions for equation (8) were computed transpiration per unit leaf area ($F_1 = E_L$), and computed Ψ_S in each soil-root layer. Each lateral root was connected to its respective bulk soil through nested rhizosphere cylinders (four in this study), where the outer cylinder was connected to the bulk soil and inner cylinder to the lateral root. The connections between roots and rhizospheres are important because there is a nonlinear drop in soil hydraulic conductance as water moves from the soil into the root. Critically low

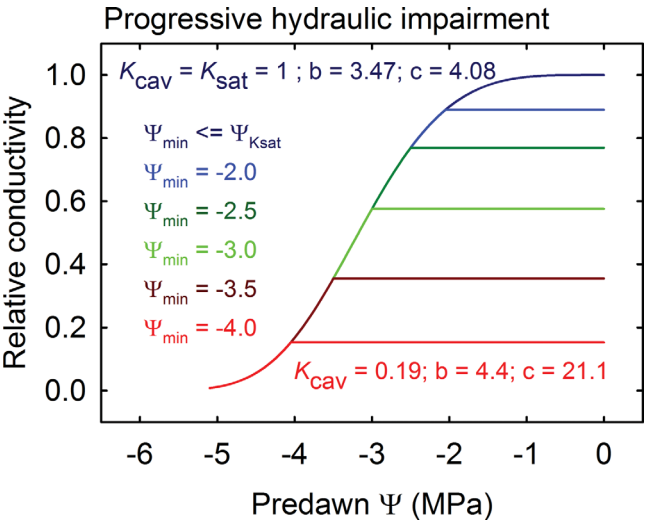

Figure 2. Relative hydraulic conductivity curves following exposure to minimum predawn water potentials (Ψ_{min}). These represent a continuum of curves that record hydraulic impairment. If a plant module fully recovers or refills with a recharge of the soil, then it follows the saturation curve (Ψ_{sat}). If refilling does not occur, then Weibull parameters b and c, and cavitated hydraulic conductivity (K_{cav}) are adjusted. Note that an exposure to a Ψ_{min} of −4.0 MPa without refilling sets relative K_{sat} to 0.19 (or 19% of the K_{sat} with no cavitation), with computed b = 4.4 and c = 21.1. Based on the initial b = 3.47 and c = 4.08, exposure to Ψ_{min} of −5.0 MPa causes hydraulic failure. If this occurs in a lateral root, then this segment of the plant is disconnected from its respective rhizosphere. If the module is a conducting stem, then the whole plant is dead from hydraulic failure. For this study, we used curves as described in *McDowell et al.* [2013].

rhizosphere conductance can ensue and must be avoided by either increasing root area relative to leaf area or reducing E_L [*Hacke et al.*, 2000]. For a given E_L and set of Ψ_S values, K_L and Ψ_L were computed along with fluxes between root elements and the rhizosphere, and hydraulic conductances and tension along the soil-to-leaf hydraulic continuum. Critical (or maximum) transpiration (E_{Lcrit}) and corresponding critical (or minimum) leaf water potential (Ψ_{Lcrit}) were computed by iteratively increasing F_1 from E_L to the point of hydraulic failure.

Once a final transpiration flux was determined, Ψ_S in each layer was updated in proportion to the rhizosphere flux. Rhizosphere fluxes followed tension gradients, and so positive rhizosphere fluxes represented water transport from soil to root, while negative rhizosphere fluxes represented water moving from root to soil. Since we assumed no capacitance for the small trees in this study, a water balance was maintained such that the sum of rhizosphere fluxes was equal to transpiration flux.

2.4. Computation of Chronic Hydraulic Impairment

The core hydraulic model [*Sperry et al.*, 1998] had the capacity to keep track of losses of K, and its benefits were previously demonstrated [*Hacke et al.*, 2000]. We present the full algorithm here to show where this is done in the coupled model. Chronic hydraulic impairment was computed by reducing the maximum hydraulic conductance and fitting a new Weibull function so that hydraulic conductance follows the nonimpaired vulnerability curve up to the new maximum conductance, K_{cav} (Figure 2). This allows the model to mimic a progressive increase in vulnerability to cavitation [*Anderegg et al.*, 2012; *Hacke et al.*, 2001] as hydraulic impairment increases in severity. K_{cav} was computed using minimum predawn water potential, Ψ_{min}, which is remembered even if there is an event that increases soil water content. TREES can be set up to prevent xylem refilling, in which case Ψ_{min} never increases, or to allow refilling, in which case Ψ_{min}, can either directly correspond to soil water tension or it can be raised when there is a sufficient increase in soil water tension. K_{cav} was computed using

$$K_{cav}(\Psi_{min}) = K_{sat}\{\exp[(-\Psi_{min}/b_{sat})^{c_{sat}}]\} \tag{11}$$

where b_{sat} and c_{sat} were model input (or nonimpaired) Weibull parameters for the vulnerability curves for each respective plant element. Then, b_{cav} and c_{cav} were computed for the impaired vulnerability curve. To do this we iteratively computed

$$K_i = \begin{cases} K_{cav}\{\exp[(-\Psi_i/b_{sat})^{c_{sat}}]\}, \Psi_i < \Psi_{min} \\ K_{cav}, \Psi_i \geq \Psi_{min} \end{cases} \tag{12}$$

and proportional loss of K as

$$P_i = 1 - K_i / K_{cav} \tag{13}$$

by decrementing Ψ_i from zero to a tension at which K_i approached 0. At the tension corresponding to the negative of parameter b we set $b_{cav} = -\Psi_i$, and iteratively solved for c_{cav} in a new vulnerability curve,

$$K_i' = K_{cav}\{\exp[(-\Psi_i / b_{cav})^{c_{cav}}]\} \tag{14}$$

that fit the nonstressed curve for tension between Ψ_{min} and Ψ_L using a least squares fit that maximized $\frac{\left(\sum_{i=1}^{k} P_i K_i'\right)^2}{\left(\sum_{i=1}^{k} P_i\right)^2 \left(\sum_{i=1}^{k} K_i'\right)^2}$.

Subsequent changes in K_L for the affected plant element were computed using

$$K_L = K_{cav}\{-\exp[(-\Psi_i / b_{cav})^{c_{cav}}]\}. \tag{15}$$

At the onset of an increase in root zone mean Ψ_S, these computations were made for each plant element to allow for differential hydraulic impairment among plant elements.

2.5. Computation of Leaf and Root Dynamics

The role of plant hydraulics was extended to control the sink strength for the allocation of carbon to growth and respiration [*Holtta et al*., 2009]. A single pool of nonstructural carbon (NSC) was defined with initial values assuming NSC represented 10% of leaf and root carbon and 4% of sapwood carbon [*Sevanto et al*., 2013], and with the total carbon pools set allometrically [*Plaut et al*., 2012]. Net photosynthesis was added to NSC. NSC was consumed by maintenance respiration at a linear rate of decline with drop in K_L, and by growth respiration in proportion to K_L squared [see *McDowell et al*., 2013 supporting information]. In addition, live leaf area, L_{live}, was computed to account for foliage mortality due to hydraulic impairment of the lateral stem:

$$L_{live} = \left[R_{R/L}^{-1} C_G (1 - f_{Cstem})\right] \cdot L_{Sp} - L_m T_D \tag{16}$$

where $R_{R/L}$ is the root-to-leaf area ratio, f_{Cstem} is fraction of carbon allocated to stem (assumed to be 0.1) [*Amthor*, 1994; *Waring and Schlesinger*, 1985], C_G is total carbon allocated to growth (gC m^{-2} ground), L_{Sp} is specific leaf area (m^2 leaf gC^{-1}), and L_m is leaf mortality rate (m^2 leaf m^{-2} ground day^{-1}), and T_D is time in days. L_m was computed as

$$L_m = \begin{cases} L_0 M, & P_L \geq 0.5 \wedge c_{ls} \leq c_{lrs} \\ P_L L_0 M, & P_L < 0.5 \wedge c_{ls} > c_{lrs} \end{cases} \tag{17}$$

where L_0 is initial leaf area index, M is unstressed leaf mortality rate, P_L is lateral stem proportional loss of conductivity, and c_{ls} and c_{lrs} are, respectively, the Weibull c parameters for the lateral stem and the lateral shallow root. We derived L_0 allometrically from site-specific data [*McDowell et al*., 2013] for individual trees by dividing total leaf area per tree by the projected crown area of the respective tree [*Mackay et al*., 2012]. Roots were hydraulically disconnected from the rhizosphere once exposed to critically low Ψ values and applying equations (11)–(15).

2.6. Simulation of Trees Under Experimental Drought

We simulated two conifer species [*McDowell et al*., 2013] from different positions along the isohydry-anisohydry continuum [*Linton et al*., 1998] exposed to experimental drought: *Pinus edulis* Englm. (piñon pine, hereafter referred to as "pine"), which is relatively isohydric [*West et al*., 2007], and *Juniperus monosperma* Englm. (Sarg.) (one-seed juniper, hereafter referred to as "juniper"), which is relatively anisohydric [*McDowell*, 2011]. Pine attempts to avoid hydraulic failure during drought by closing stomata and hydraulically disconnecting its roots from the rhizosphere, and it grows relatively shallow roots that can reconnect during summer monsoon events [*Plaut et al*., 2013; *West et al*., 2007]. Juniper relies less on shallow roots, and keeps stomata open during drought, allowing for progressive mortality in the canopy [*West et al*., 2007]. The data we used for these species were: sap flux for transpiration, leaf gas exchange to determine

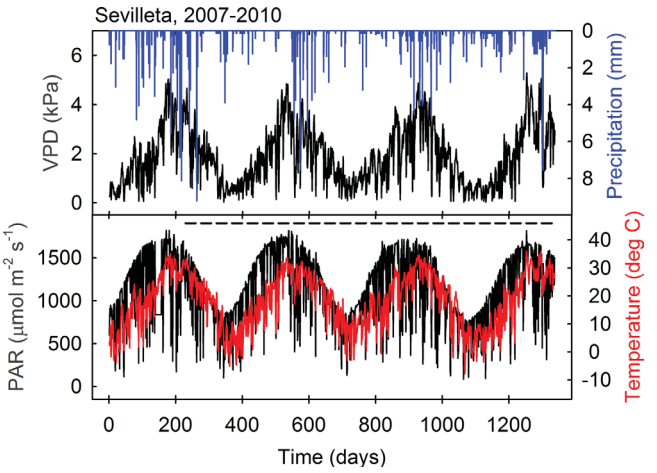

Figure 3. Shown are primary meteorological inputs to TREES for the pine-juniper experimental drought study [*McDowell et al*., 2013]. Vapor pressure deficit (VPD), photosynthetically active radiation (PAR), and temperature shown are midday values. Precipitation is shown for every event. The dashed, horizontal line represents the period during which precipitation was reduced by 45% at the study site and in the input precipitation to TREES. The precipitation values are shown with the 45% reduction.

V_{cmax} and φ for photosynthesis, water potential data [*Pockman and McDowell*, 2014c], allometry to scale tree properties (i.e., leaf area index, plant carbon pools, and root lateral lengths), site-specific micrometeorology (i.e., air temperature, humidity, wind speed, precipitation, and photosynthetically active radiation) [*Pockman and McDowell*, 2014b], and soil temperature [*Pockman and McDowell*, 2014a] as reported in a number of publications [*Gaylord et al*., 2013; *Limousin et al*., 2013; *McDowell et al*., 2013; *Plaut et al*., 2012, 2013]. We also used visual signs of chronic hydraulic impairment of the canopy (i.e., percent canopy browning). Mortality in piñon pine is associated with rapid (4 weeks or less) change in needle color from green to orange [*Adams et al*., 2009; *Breshears et al*., 2009; *Gaylord et al*., 2013; *Plaut et al*., 2012], and relatively slow (over years) in juniper based on loss of leaf area [*Gaylord et al*., 2013]. Parameter inputs are summarized in Table 1 and primary meteorological inputs are shown in Figure 3. Based on previous simulations conducted at the site [*McDowell et al*., 2013] and the goal of comparing strong drought responses, we selected one average drought pine and one drought juniper (see supporting information).

For both trees we ran simulations with 30 min time steps from 1 January 2007 to the respective dates when the trees were observed to have died, which was mid-August 2008 for the pine (565 days of simulation) and mid-August 2010 for the juniper (1330 days). To mimic the experimental drought, we reduced all precipitation events by 45% beginning 15 August 2007. For both trees we ran one simulation with xylem refilling triggered at each precipitation event to allow the trees to maintain equilibrium with soil water status, and a second simulation with no xylem refilling to maintain chronic hydraulic impairment over successive soil drying periods. In a third simulation for pine, we forced hydraulic disconnect of the shallow and middle lateral roots from their respective rhizospheres by exposing them to predawn water potential of −8 MPa. This was done on day 270 for the shallow root and day 500 for the middle root, respectively timed to occur at the end of the monsoon in year 1 and in late spring in year 2, at times when one would have expected root refilling or reconnection with the rhizosphere and the sap flux data suggests that this did not happen [*Plaut et al*., 2013].

2.7. Simulation Experiments With Root Structural Adjustments

We evaluated the effects of pine versus juniper hydraulic traits on potentially optimal root architectures. Parameter adjustments are shown in Table 1. Specifically, we evaluated sensitivity of modeled hydraulic traits and gas exchange using pine and juniper vulnerability curves and changes in root distribution with depth, rhizosphere flux density as represented with $R_{R/L}$, and soil hydraulic parameters. In a first set of simulations, we eliminated micrometeorological trends by taking a representative day from the first week of July 2007. This "day" had an average midday D of 3.0 kPa and zero precipitation. It was replicated to produce a 110 day meteorological driver file in which two 10 mm rainfall events were added, one on day 30 and a second on day 80. This produced a micrometeorology input that allowed us to more cleanly visualize the plant hydraulic responses to soil water. We employed two sets of vulnerability curves (pine, juniper) [*McDowell et al*., 2013], two root profiles (uniform root area with depth, declining root area with depth), and eight root-to-leaf area ratios ($R_{R/L}$ = 0.25, 0.5, 1.0, 1.5, 2.0, 3.0, 4.0, and 5.0), as well as two soil textures (clay content 6% and 10%) at a $R_{R/L}$ of 3.0 with declining root area with depth. All other model inputs were held constant between simulations. Initial Ψ_S was set at −0.8 MPa. Xylem was not allowed to refill. Between events the mean soil water content declined monotonically via transpiration with zero evaporation. We compared

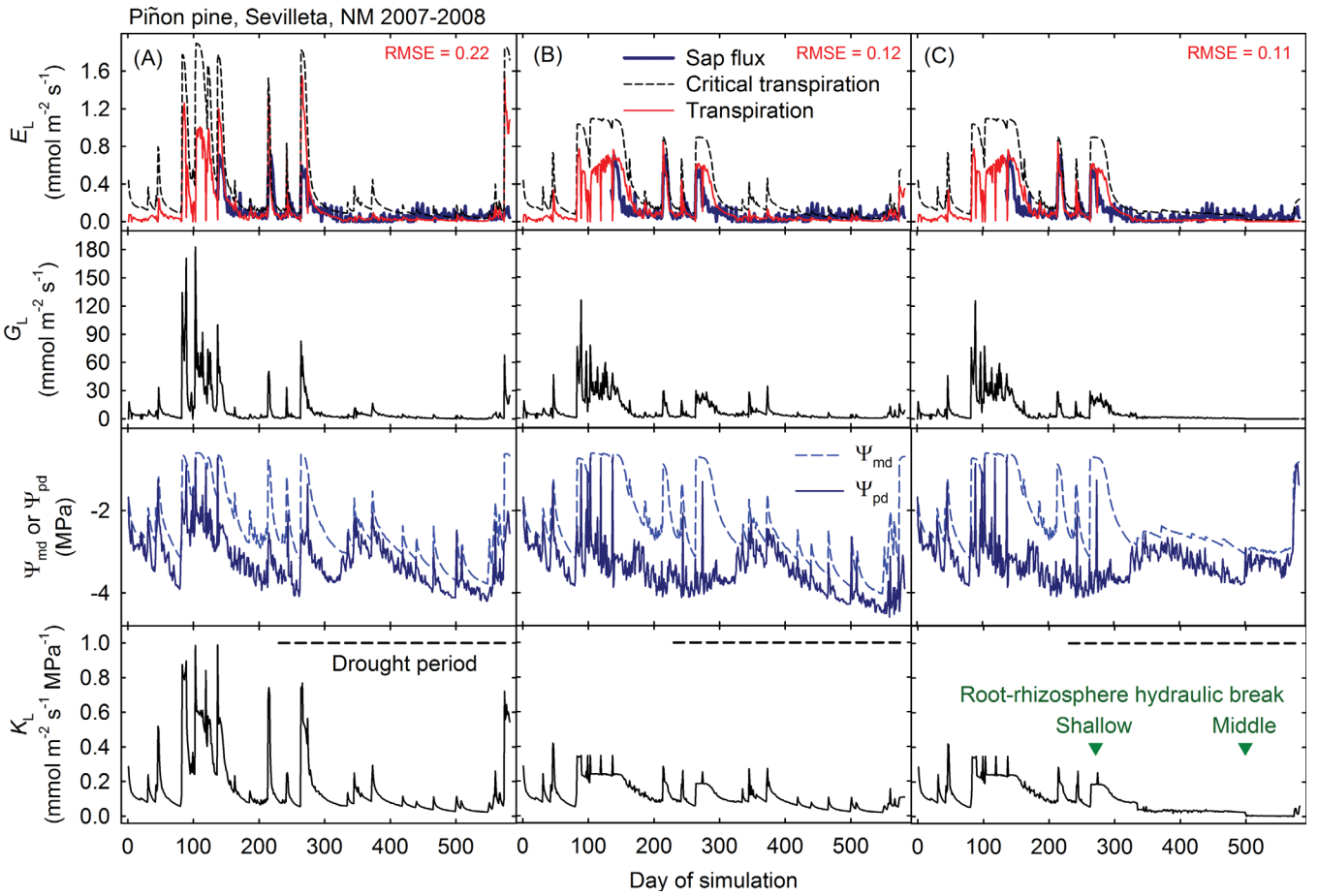

Figure 4. Simulation of midday transpiration (E_L), midday stomatal conductance (G_L), predawn (Ψ_{pd}) and midday (Ψ_{md}) water potentials, and whole plant hydraulic conductance per unit leaf area (K_L) for (a) cavitation refilling, (b) no refilling, and (c) no-refilling with hydraulic disconnect of shallow and middle root modules. Day 0 is 1 January 2007. Drought was initiated on day 230. Green arrows indicate where the shallow and middle absorbing roots were disconnected from their respective rhizospheres. Root mean square error (RMSE) is between transpiration and sap flux for the respective simulations.

midday hydraulic parameters (K_L, Ψ_S, Ψ_{md}) and G_L on days 2, 31, and 81 corresponding to 1 day after initialization and 1 day after each precipitation event, respectively.

Investment in roots can benefit a plant by increasing water (and nutrient) access, but it also costs carbon to both construct and maintain the roots. Consequently, a second set of simulation experiments was used to show tradeoffs in carbon uptake and water use across different values of $R_{R/L}$. We ran simulations for each tree for $R_{R/L}$ values between 1 and 5 using the full micrometeorological data, with roots confined to the top 70 cm in one set of simulations and a 105 cm in a second set. We then computed means of gross primary production (GPP), GPP—root respiration, transpiration, and hydraulic parameters for pre-drought and drought periods.

3. Results

3.1. Simulation of Tree Response to Drought

There was a pronounced monsoon in 2007 (centered on day 200) and weaker monsoon in other years in part because of the 45% experimental reduction in precipitation (Figure 3). Given these precipitation patterns, one would anticipate recovery of plant hydraulic status following monsoon events assuming plants were able to refill. In general, the driest periods were April–June, and by implication hydraulic impairment was anticipated prior to monsoon.

Figures 4 and 5 show simulated and measured E_L, and simulated G_L, predawn and midday Ψ_L, and K_L. Simulated E_L did not resemble seasonal sap flux dynamics when xylem refilling was enabled (Figures 4a and 5a). In particular, there was an erroneous response to monsoons, particularly in 2008 for pine, and in 2008, 2009,

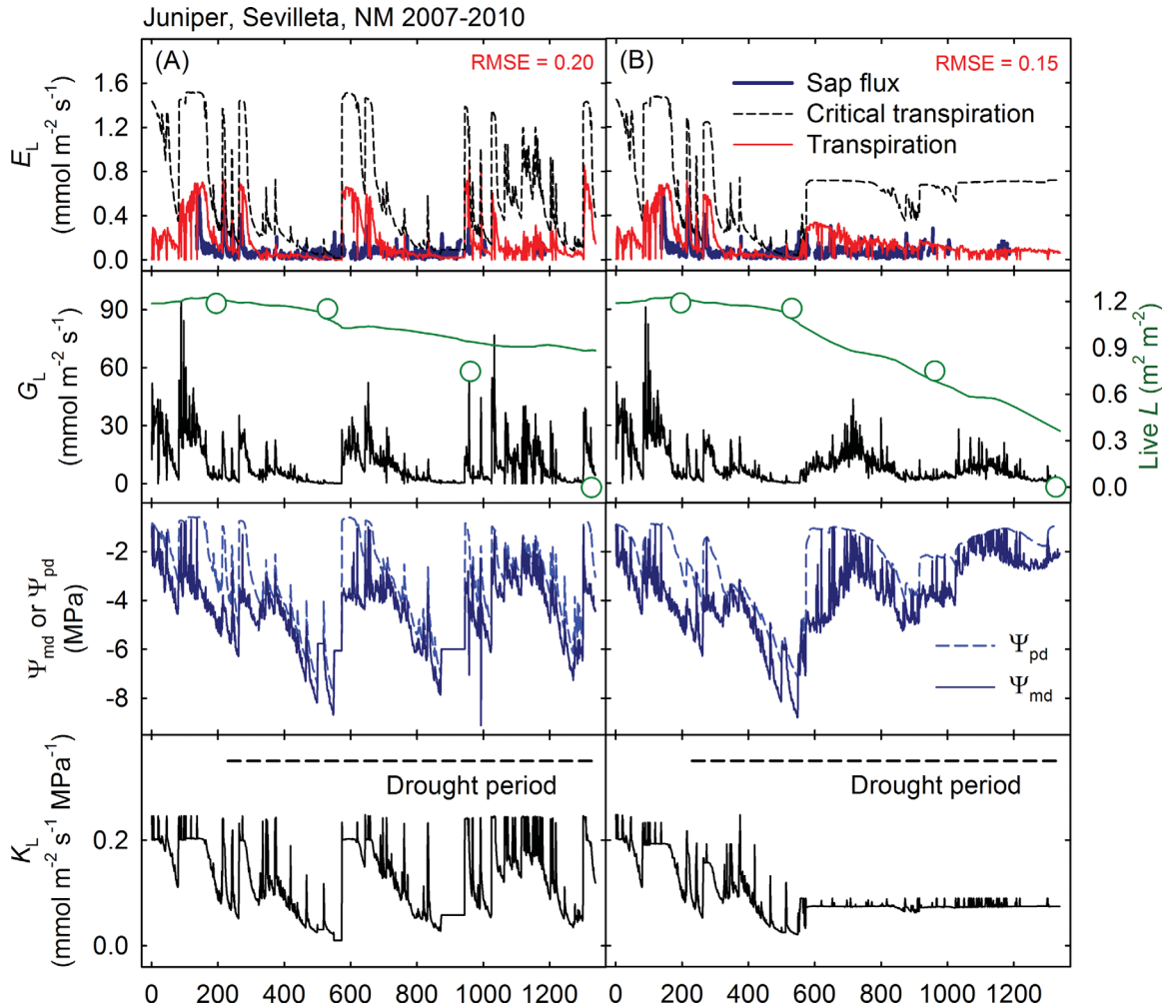

Figure 5. Shown are simulation of midday transpiration (E_L), midday stomatal conductance (G_L), live leaf area index (L), predawn (Ψ_{pd}) and midday (Ψ_{md}) water potentials, and whole plant hydraulic conductance per unit leaf area (K_L) for juniper. Day 0 is 1 January 2007. Drought was initiated on day 230. Column (a) assumes refilling while (b) assumes no refilling of embolized xylem. The red lines are sap flux measurements scaled to a temporally constant L of 1.19 m^{2}m^{-2}. Green open circles represent observed live L. Root mean square error (RMSE) is between transpiration and sap flux for the respective simulations.

and 2010 for juniper. When there was no modeled xylem refilling, simulated E_L more closely followed the sap flux seasonal dynamics and root mean square error (RMSE) declined (Figures 4b and 5b). E_L predictions for pine were further improved toward the end of the simulation when the shallow and midlevel lateral roots were disconnected from their respective rhizospheres (Figure 4c). The effect of hydraulic impairment on a declining L was also expressed in juniper (Figures 5b versus 5a), but not in pine (not shown as there was no change in L). In fact, the pine tree was observed in the field to change needle color from green to orange over a 3 week period culminating in mortality. TREES does not have the capacity to make such predictions. But TREES predicted the observed juniper canopy loss (Figure 5b, Live L).

The pine allowed for smaller midday Ψ_L departure from predawn values during drought compared to juniper (about 0.5 versus 1.0 MPa), as expected from pine's isohydric regulation of Ψ_L. There was some compensation (Figure 4b) in midday Ψ_L for the lower K_L values. Juniper allowed Ψ_L to progressively move with Ψ_S during drought. Simulated Ψ_L without refilling explained 70 and 80 percent of pine, and 82 and 77 percent of juniper predawn and midday Ψ_L, respectively (Figures 6c and 6d). These were notably improved over Ψ_L values simulated with refilling (Figures 6a and 6b), particularly for pine. The model slightly underestimated predawn Ψ_L for juniper.

3.2. Simulation Experiments With Root Structural Adjustments

The isohydric species G_L recovered less with each successive dry-down compared to the anisohydric species G_L (Figure 7). The decline in Ψ_L was limited by stomatal closure in both species, but was more pronounced

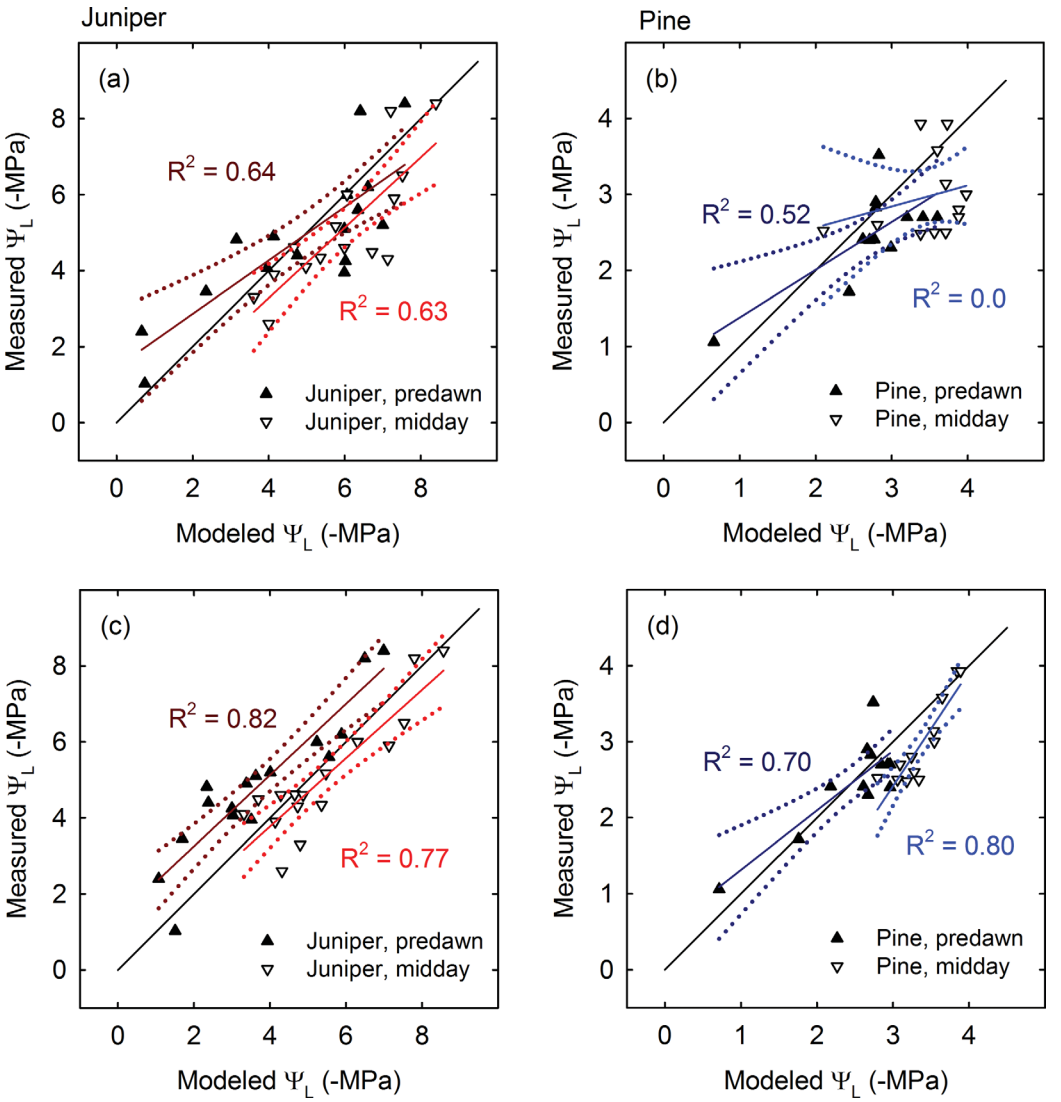

Figure 6. Modeled versus measured predawn and midday leaf water potentials for pine and juniper. Simulations are with refilling (a, b) and no refilling (c, d) of embolized xylem for both pine and juniper, and hydraulic disconnect of shallow and midlevel roots in pine in late-2007 and mid-2008, respectively. All regressions (solid red or blue) are significant at $p < 0.005$ except midday pine with refilling (c). Solid black lines are the one-to-one and dotted lines represent the 95% prediction interval.

for the isohydric species. For example, just before the day 80 precipitation event the isohydric species approached stomatal closure at Ψ_S of about -2.5 MPa, while the anisohydric tree did not approach stomatal closure until Ψs was less than -5.0 MPa. The isohydric G_L was lower and recovered less in response to precipitation when soils had higher clay and silt content (Figures 7b and 8). But this change in soil texture was insufficient to elicit a response from the anisohydric G_L.

G_L increased monotonically with $R_{R/L}$ for the anisohydric juniper and had a saturating response for the isohydric pine under predrought conditions for a uniform distribution of roots with depth (Figure 9), reflecting an increase in water extraction capability. Under unimpaired conditions the isohydric species with variable root distribution had a declining G_L at $R_{R/L} > 2$ (Figure 9b). Under impaired conditions all species-root combinations also showed nonmonotonic changes in G_L with increasing $R_{R/L}$. The reason for this is that maximizing cumulative root water uptake resulted in a greater decline in rhizosphere flux and thus a decline in K_L that could not be compensated for with a decline in Ψ_L. Alternatively, the anisohydric response to a decline in K_L associated with reduced rhizosphere soil water was to continue to drop Ψ_L. We also note that, for the isohydric species cavitation took place in the xylem at $R_{R/L} > 2$, while for the anisohydric species

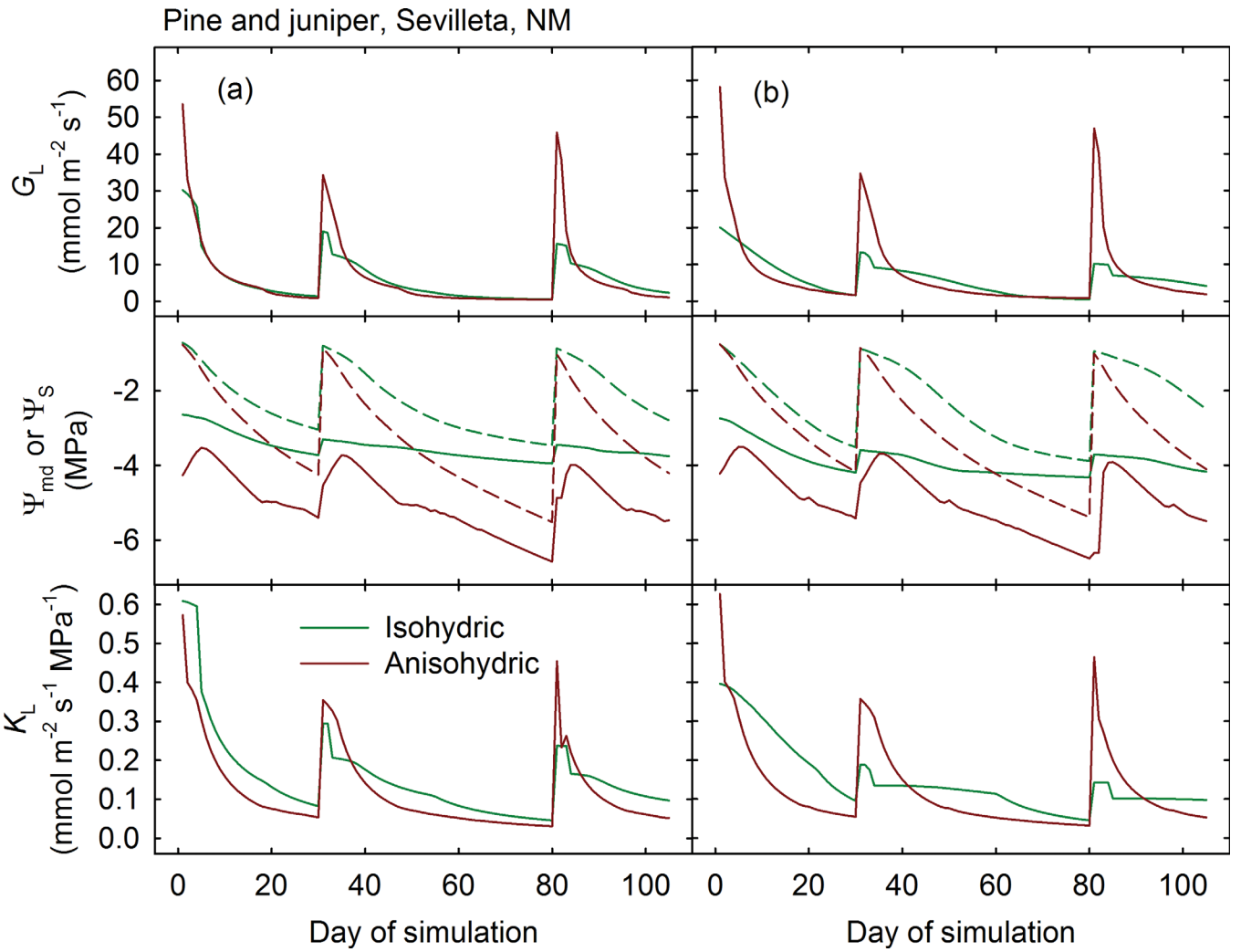

Figure 7. Shown are plant hydraulic responses to predrought (no cavitation) and two post drought (cavitated) states for both isohydric pine and anisohydric juniper. The only input differences between pine and juniper simulations in these plots are their respective vulnerability to cavitation curves. The simulations used a root-leaf area ratio of 3 and a declining root area with depth. In column (a) the soil texture was that observed at the study site (clay = 6%, silt = 40%). In (b) the soil texture was finer (clay = 10%, silt = 44%). Shown are midday stomatal conductance (G_L), midday leaf water potential (Ψ_{mid}) (solid), soil water potential (Ψ_S) (dashed), and midday whole-plant hydraulic conductance (K_L). Simulated trees were exposed to a soil moisture drawdown followed by a single 10 mm rainfall event (day 30). The trees were then exposed to a second soil moisture drawdown for 50 days, followed by a second single 10 mm rainfall event.

cavitation took place in the rhizosphere at $R_{R/L} > 3$. These results are an emergent response of simulating coupled canopy flux processes and both hydraulic limitations in the soil and vulnerability to cavitation in the xylem.

K_L was responsive to changes in root distribution and $R_{R/L}$ for predrought and postdrought states, and to root distribution for predrought states associated with sum of root path length and thus total hydraulic resistance. The effects of these responses of K_L on G_L were clear for the isohydric tree, but with anisohydry the root distribution had a negligible effect on G_L. The responses of hydraulic parameters to $R_{R/L}$ also differed between tree types. For the isohydric tree K_L (and G_L) peaked at a $R_{R/L}$ of 2, whereas for the anisohydric tree K_L peaked around a ratio of 1.5, but G_L did not reach a peak for predrought conditions and peaked at a $R_{R/L}$ of 3 following drought. While K_L generally declined for both trees at high root density, the anisohydric tree was able to progressively decrease Ψ_L as higher values of root area resulted in increasing water extraction. Thus, anisohydry enabled a higher G_L per unit of K_L. Alternatively, the isohydric tree showed no decline in Ψ_L with increasing rooting area. These isohydry-anisohydry results are emergent from the model rather than prescribed, demonstrating the power of completely coupling the canopy and full rhizosphere-plant hydraulics.

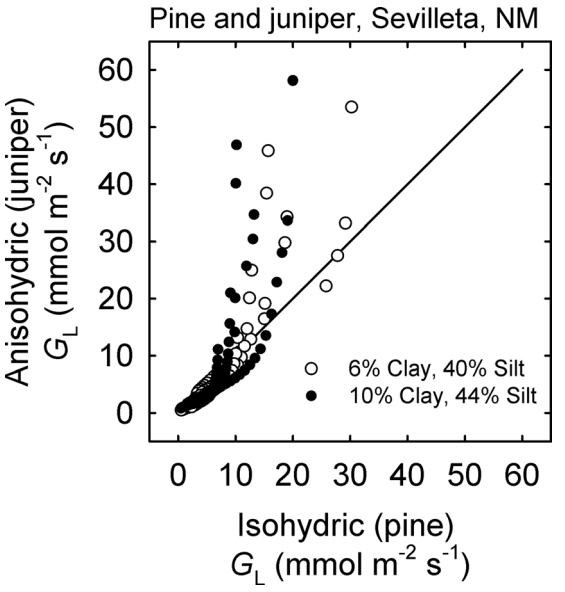

Figure 8. Isohydric G_L is plotted versus anisohydric G_L. Simulated trees were exposed to a soil moisture drawdown followed by a single 10 mm rainfall event (day 30). The trees were then exposed to a second soil moisture drawdown for 50 days, followed by a second single 10 mm rainfall event.

Both water loss and carbon uptake increased with $R_{R/L}$ (Figure 10). GPP peaked at the highest root area for both species and periods. When taking into consideration costs of having more root (maintenance respiration), or alternatively less L for a fixed carbon uptake, neither species showed an increase in net carbon at $R_{R/L}$ greater than 3. Pine showed little change in water use with $R_{R/L}$, and juniper increased its predrought water use and decreased drought water use at higher root areas. Pine and juniper both increased Ψ_S-Ψ_L with increasing $R_{R/L}$ for both predrought and drought periods. Pine percent loss of conductivity (PLC) decreased from $R_{R/L}$ of 1 to 2 and then increased at higher $R_{R/L}$, while juniper PLC increased monotonically with $R_{R/L}$. Predrought and drought pine averaged 50% and 80% PLC, respectively, and predrought juniper averaged 10% PLC. Drought juniper showed an increase in PLC with $R_{R/L}$ and exceeded 50% at an $R_{R/L}$ of 3 or higher. Root depth minimally affected pine fluxes and hydraulic parameters, while increasing predrought juniper fluxes and

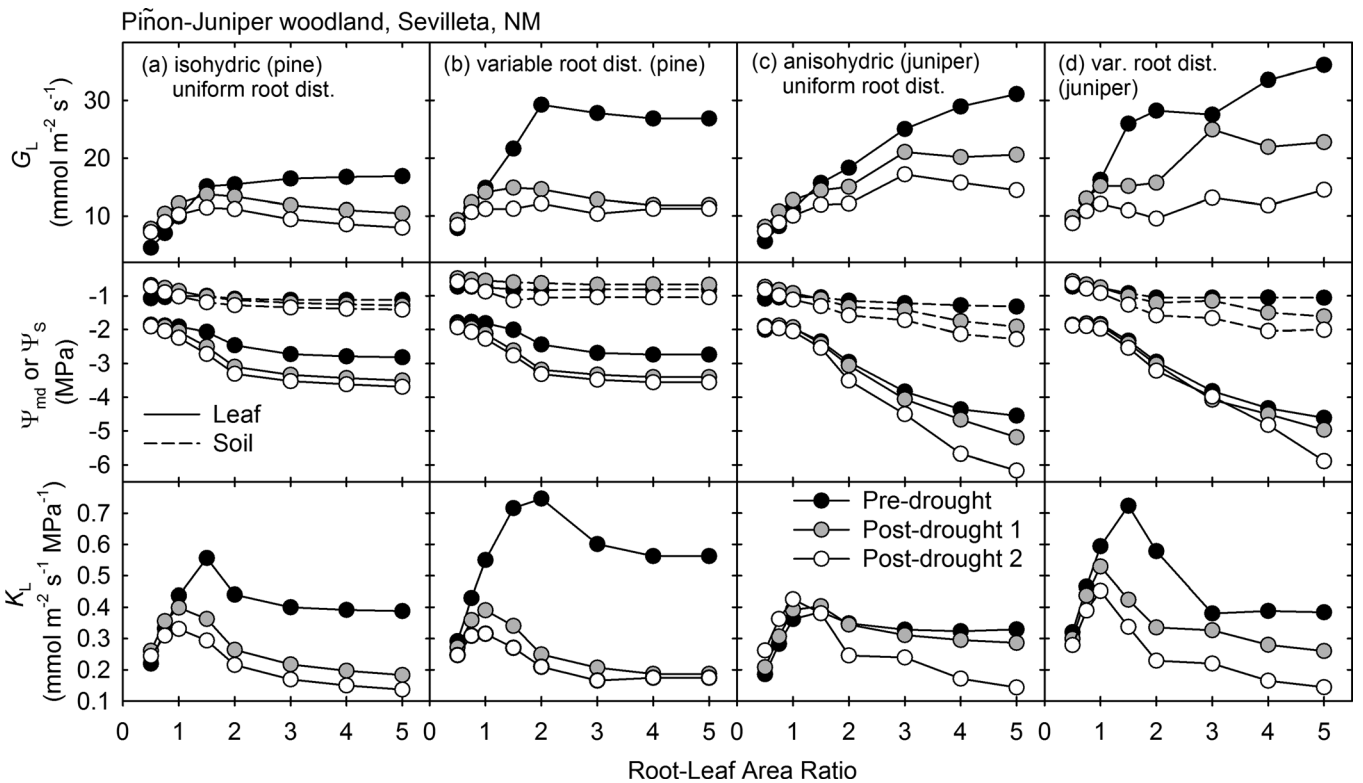

Figure 9. Plant hydraulic responses to changes in root distribution and root-leaf area ratio for predrought (saturated K_L) and two post drought (impaired) states. Shown are midday stomatal conductance (G_S), leaf water potential (Ψ_{mid}), soil water potential (Ψ_S), and whole-plant hydraulic conductance (K_L). Simulated trees were exposed to soil moisture drawdown followed by a single 10 mm rainfall event (day 30). The trees were exposed to a second soil moisture drawdown for 50 days, followed by a second single 10 mm rainfall event. The predrought plots are from day 2, post drought 1 plots are from day 31 of simulation, and post drought 2 plots are from day 81. Columns (a) and (b) were simulated for vulnerability to cavitation curves for the isohydric (pine) species. Plots in columns (c) and (d) are for anisohydric case based on juniper. Columns (a) and (c) assume uniformly distributed root area with depth to 70 cm, while (c) and (d) assume a declining root area with depth to 70 cm. No other model inputs were altered.

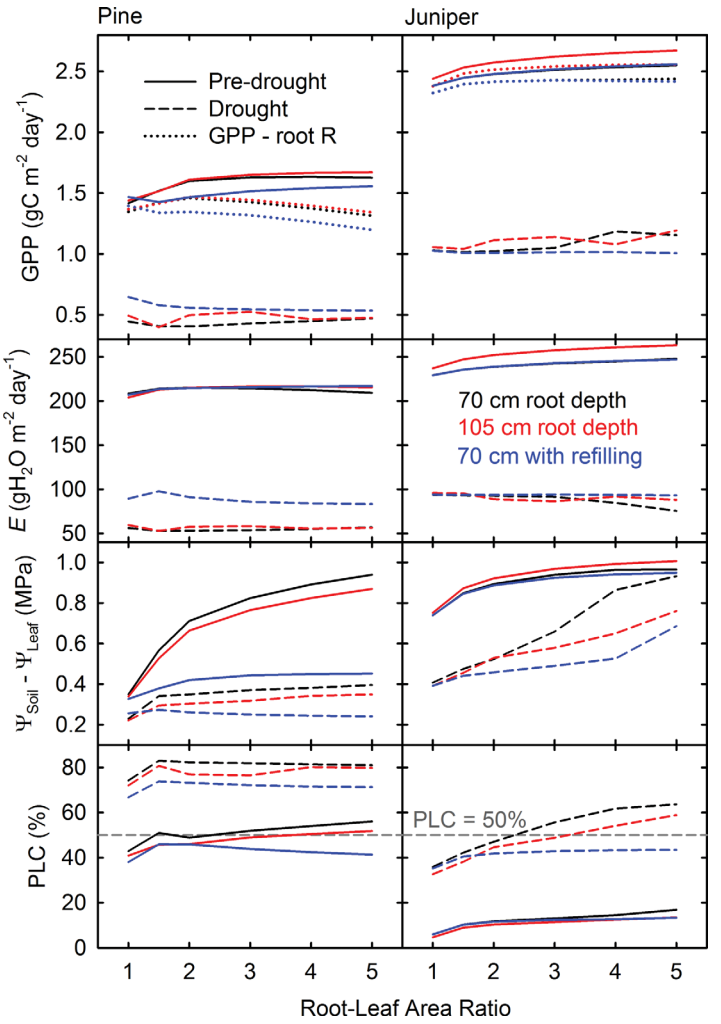

Figure 10. Plant flux and hydraulic responses to root-leaf area ratio for predrought and drought periods for pine and juniper, for roots confined to 70 cm (black lines) and 105 cm (red lines) depth without refilling, and 70 cm with refilling (blue lines). Plots show mean gross primary production (GPP), GPP minus root respiration (R), transpiration (*E*), difference between soil (Ψ_{Soil}) and leaf water potential (Ψ_{Leaf}), and percent loss of conductivity (PLC). For both pine and juniper, the predrought period was 230 days in length starting 1 January 2007. The pine simulations ran to August 2008, and the juniper simulations ran to August 2010.

reducing water stress during the drought period. Distributing root area over greater depth did not change the overall patterns of flux and hydraulic responses. But with xylem refilling predrought GPP was generally lower, predrought E_L did not change, drought pine GPP and E_L increased, and drought juniper GPP decreased compared to simulations without refilling.

4. Discussion

4.1. Simulation of Trees to Experimental Drought

TREES accurately predicted E_L and Ψ_L over multiple years of simulation of predrought and drought after initialization with hydraulic parameters estimated during a well-watered condition. Within the limitations of available field data, e.g., lack of belowground data, we would not anticipate a big improvement in simulation accuracy even with sophisticated calibration [*Mackay et al.*, 2012], regardless of which trees had been selected from the study site (see supporting information). For example, in the present study there was no evidence of a need for xylem refilling in the simulations. For juniper, the model was able to show that the role of declining water status and greater hydraulic stress in the stem relative to the root after extended drought explained much of the observed mortality in the juniper canopy (Figure 5). Differential effects of drought timing and duration on live foliage areas due to progressive cavitation could help explain why

junipers in some studies showed higher PLC than pines [*McDowell et al*., 2008] while the reverse was shown in other studies [*McDowell et al*., 2013]. The simulation results for pine supported the hypothesis that trees of this species at the study site disconnected their lateral roots in the shallower layers (Figure 4), as shown by leaf water potentials tracking deep root zone soil water potentials in the study by *Plaut et al*. [2013].

4.2. Optimal Root Structural Adjustments

It has been hypothesized that trees optimize $R_{R/L}$ to achieve sufficient water extraction with respect to root investment [*Ewers et al*., 2000; *Hacke et al*., 2000]. In fact, this idea forms the underlying logic in the earliest tree carbon allocation models [e.g., *Running and Gower*, 1991]. Such adjustments have indeed been previously shown with plant hydraulic modeling [*Ewers et al*., 2000; *Magnani et al*., 2002]. In this study we addressed root distribution through the three soil layers, and root area in each layer as a function of $R_{R/L}$. Our modeling analysis suggested that $R_{R/L}$ represented a trade-off between potential for water extraction to support net carbon gain, and a need to conserve water during drought. In particular, higher $R_{R/L}$ resulted in greater cumulative water extracted from the soil early in the simulation. This drove down soil moisture faster, thus forcing a decline in G_L, which in turn limited photosynthesis. Moreover, it shortened the time to onset, and increased the intensity, of hydraulic dysfunction, which started to develop even before the experimental drought period in our simulations (Figures 4 and 5). The impact of this on the plant hydraulics is seen in the larger diurnal range in tension (Figure 10, third row plots) and PLC (Figure 10, fourth row plots). This might be acceptable if there was a clear benefit of carbon gain, which is clearly not the case (Figure 10, first row plots). Indeed, there are diminishing returns of carbon gain at higher $R_{R/L}$ because GPP and total water extraction either do not increase (isohydric case) or increase at a small rate compared to the cost of supporting the added roots (anisohydric case). On the basis of predrought G_L, juniper appeared to be able to take advantage of a $R_{R/L}$ of 5 giving it high potential to extract water. But both predrought carbon uptake efficiency and drought water uptake efficiency suggest that a more conservative $R_{R/L}$ of 3 is reasonable. While higher $R_{R/L}$ favors greater water extraction in the short-term, over the duration of extended droughts, cavitation in the rhizosphere due to excessive cumulative water extraction at higher $R_{R/L}$ would set up early severe drought stress even for the anisohydric tree. In effect, the need for conservation of water for survival through extended droughts would favor a reduced upper limit on $R_{R/L}$ for both isohydric and anisohydric species.

The isohydric species had optimal function for both water and carbon at a more conservative $R_{R/L}$ of 2. We suggest that there is little advantage to investing in higher $R_{R/L}$ for the isohydric species, as there is rapid stomatal closure during drought. Alternatively, the anisohydric tree benefits from higher $R_{R/L}$ because it can continue to obtain carbon as it extracts soil moisture to progressively drier levels. This difference would provide juniper with an evolutionary advantage since it could minimize root competition by cooccurring species by prolonging periods of low water potentials. Thus, cooccurrence of pine with juniper could be attributed in part to pine's allocation to shallower roots compared to juniper and an ability to hydraulically disconnect roots from the rhizosphere to conserve water [*Plaut et al*., 2013; *West et al*., 2007].

The functional trait differences between species shown in this simulation analysis demonstrate the sensitivity of stomatal conductance to vulnerability to cavitation. Under predrought conditions a similar level of stomatal conductance can be achieved with both species through adjustments in root architecture. No adjustments in the root architecture, however, prevented hydraulic impairment in the pine. The implication is that pine could adjust its root architecture to emphasize shallow roots over deeper roots to take advantage of smaller rainfall events and avoid the risks of investing in deeper roots that benefit most from infrequent, deeply penetrating precipitation events. Our simulations suggest no such strategy is needed with juniper since its reduced vulnerability to cavitation would allow it to rely less on small precipitation events and hold out for infrequent, larger precipitation events to relieve water stress. Such results are emergent, not prescribed, properties of connecting gas exchange to plant hydraulics with vulnerability to cavitation. Moreover, these functional traits are consistent with observations made of these species [*Plaut et al*., 2013; *West et al*., 2007] and others in the U.S. southwest [*Hultine et al*., 2006], demonstrating the power of linking simulations of stomatal conductance to vulnerability to cavitation along with carbon metabolism and transport. These results are not intended to exclude scenarios in which plants are adapted to grow deep roots to access groundwater, and such systems could also be explored with the addition of a groundwater component in TREES.

4.3. Limitations of the Model

As with any model, TREES has elements that could be improved upon in future development. The model presently does not account for competition and facilitation between cooccurring plants for resources, such

as the comingling of roots. Competition for water may play an important role in codevelopment of pine and juniper at the study site, and generally for cooccurring species in other sites. It is notable that these two species tend to be found comingled in clusters, suggesting perhaps a mutualistic relationship at some point in their lifespan. Although not explicitly defined in the model our simulation findings supported shallow-root dependence in pine and less of a depth-dependence of juniper roots. With the addition of both shared and unshared root spaces, it may be possible to expand these results to consider the role of root competition on local adjustments to $R_{R/L}$ and root vulnerability.

We assumed that tree height was not an important factor in the hydraulics for the short-statured trees ($<$ 4m) at this site. However, it is not necessary to exclude height from the computation of G_S, since it is possible to include it as a rate-limiting factor in the numerical solution, by adjusting downward G_{Sref}, or explicitly including a height term in the equation set [*Novick et al*., 2009]. Moreover, scalable terms that account for competing mechanisms such as changes in xylem architecture including tapering [*McCulloh and Sperry*, 2005] and adjustments for tree height [*Domec et al*., 2008] could also be considered in future model development.

The model currently provides a way to indicate when xylem refilling should occur. This is enabled with a flag field in the input driver file, and so refilling can be turned on for specific time steps. It would be better to have an automated way to enable or disable refilling, such as using a threshold increase in soil water content. Moreover, it would be ideal to have a mechanism that allowed for refilling in particular plant structures based on some threshold of cavitation. We believe such general mechanisms will at some point be of practical use in models, but as yet the empiricism to justify it is lacking.

The carbon cycle components in TREES largely resemble those of other models and include some empiricism [*Franklin et al*., 2012]. It includes a simple setup with a single pool of NSC from which maintenance respiration is removed. The remaining carbon is allocated to leaf, root, and stem components. Although we assumed a stem proportion of carbon allocation of 0.1 in this study this is not hard-coded into the model, and so it can be adjusted for other studies. One possibly unique addition in TREES is computation of carbon uptake and allocation based on plant hydraulic limitations. As such, it is potentially feasible to include the full feedback between carbon allocation and the structure and function of the root, stem, and canopy, thus providing long-term bidirectional connections between carbon availability and carbon allocation. These connections are not yet fully realized in TREES, but represent future development. Moreover, while the emphasis in the model has been on rate limitation due to soil-plant hydraulics, light limitation was not a consideration here but is included in TREES [*Loranty et al*., 2010a; *Mackay et al*., 2012]. At present TREES lacks specific functions for computing nutrient limitation, a known mechanism of hydraulic adjustment [*Ewers et al*., 2000], or consequent declines in V_{Cmax} during severe drought [*Wilson et al*., 2000]. These feedbacks will be considered in future model development. Also, since the full set of mechanisms causing tree mortality is as yet unknown TREES is unable to capture mortality from drought. This too remains to be developed.

The observed coordination between stomatal regulation and underlying hydraulics shown here suggests the possibility of simplifying the G_L estimation by coupling it directly to an $E(\Psi)$ supply function [*Sperry and Love*, 2015]. Such a simplification would likely ease the migration of our approach into larger-scale models, such as earth system models, by reducing the number of steps in the solution presented in section 2.2.

4.4. Broader Implications

TREES takes a direct approach to computing gas exchange as a function of competing demands for carbon and water. This notion of coupling plant hydraulics to constrain stomatal conductance and photosynthesis is not new. Some existing integrated models use plant hydraulics to compute a stress factor on stomatal conductance [*Bohrer et al*., 2005; *Janott et al*., 2010; *Manzoni et al*., 2014], to augment semiempirical equations of stomatal control coupled to photosynthesis [*Da Silva et al*., 2011; *Domec et al*., 2012; *Quijano et al*., 2012; *Tuzet et al*., 2003], or to maximize photosynthesis while maintaining leaf water potential above a minimum [*Williams et al*., 1996]. A notable departure of TREES from these models is the coupling of stomatal conductance to chronic hydraulic impairment in the xylem and carbon metabolism explicitly rather than empirically. This enables TREES to build in memory or transient responses to drought rather than equilibrating plant water status with soil water status, a mechanism that *Manzoni et al*. [2014] recently suggested as needed in models. In TREES, this memory of impairment is expressed differentially in each part of the plant,

enabling the model to simulate progressive impairment of roots at different depths as shown here for pine, or progressive failure of the canopy, e.g., for juniper, even through periods of soil water recovery.

Our results show the benefits of modeling such transience of plant hydraulic traits for understanding plant responses to drought because they reveal emergent behavior of the isohydric and anisohydric species without prescribing it. For isohydric this included water loss avoidance (i.e., stomatal closure, hydraulic isolation) and soil water depletion avoidance (i.e., low $R_{R/L}$), and for anisohydric this included sacrificing the canopy in favor of sustained carbon acquisition (i.e., leaf abscission, higher $R_{R/L}$ to extract more soil water). It would be interesting to compare our results to those of models that optimize plant behavior as a response to long-term average water status [*Gustafson et al*., 2014], as these models might miss short-term dynamics while arriving at similar conclusions about the probability of tree mortality over longer periods [*Anderegg et al*., 2012; *Sala et al*., 2010].

By incorporating chronic hydraulic impairment, next generation models could be used to help understand links between plant water status and carbon assimilation and transport within the plant, improve the conceptual basis for adjusting root distributions and root-to-leaf area ratios, select for plant traits in climate change modeling, and interpret carry-over effects of drought on long term ecosystem resource utilization. There is growing evidence of coordination between these mechanisms and plant hydraulics [*Brodribb et al*., 2002; *Brodribb and Holbrook*, 2006; *McDowell et al*., 2008; *Sala and Hoch*, 2009; *Tardieu and Davies*, 1993]. Models could predict transient responses of plant traits to external forcing such as climate warming, drought, and disturbance, and consequently predict changes in the hydrologic cycle where historical data are an unreliable proxy for future conditions. As a new generation of dynamic models emerges, there will be increased need to consider ecosystem dynamics offered by tracking chronic hydraulic impairment and not just resource optimization as a driver of ecosystem states [*McDowell et al*., 2011].

Acknowledgments
Development of TREES was partially supported by grants from the National Science Foundation (EAR-0405306, EAR-0405381), Department of Energy Office of Biological and Environmental Research, National Institute for Climatic Change Research (NICCR) Midwestern region sub-agreement 050516Z20, and the College of Arts & Sciences at the University at Buffalo. The long-term experimental data used in this study were supported by the U.S. Department of Energy Office of Science (BER). The statements made in this manuscript reflect the views of the authors and do not necessarily reflect the views of the funding agencies. We are grateful to Simone Fatichi and two anonymous reviewers whose comments helped improve the manuscript. Data used in this manuscript are available from the LTER network [see *Pockman and McDowell*, 2014a, 2014b, 2014c]. TREES can be obtained by contacting the first author.

References

Adams, H. D., M. Guardiola-Claramonte, G. A. Barron-Gafford, J. C. Villegas, D. D. Breshears, C. B. Zou, P. A. Troch, and T. E. Huxman (2009), Reply to Leuzinger et al.: Drought-induced tree mortality temperature sensitivity requires pressing forward with best available science, *Proc. Natl. Acad. Sci. U. S. A.*, *106*(38), E107–E107.

Amthor, J. S. (1994), Plant respiratory responses to the environment and their effects on the carbon balance, in *Plant-Environment Interactions*, edited by R. E. Wilkinson, pp. 501–554, Marcel Dekker, N. Y.

Anderegg, W., J. Berry, and D. Smith (2012), The roles of hydraulic and carbon stress in a widespread climate-induced forest die-off, *Proc. Natl. Acad. Sci.*, *109*, 233–237.

Berry, J. A., D. J. Beerling, and P. J. Franks (2010), Stomata: Key players in the earth system, past and present, *Curr. Opin. Plant Biol.*, *13*(3), 232–239.

Blackman, C. J., T. J. Brodribb, and G. J. Jordan (2009), Leaf hydraulics and drought stress: Response, recovery and survivorship in four woody temperate plant species, *Plant Cell Environ.*, *32*(11), 1584–1595.

Bohrer, G., H. Mourad, T. A. Laursen, D. Drewry, R. Avissar, D. Poggi, R. Oren, and G. G. Katul (2005), Finite element tree crown hydrodynamics model (FETCH) using porous media flow within branching elements: A new representation of tree hydrodynamics, *Water Resour. Res.*, *41*, W11404, doi:11410.11029/12005WR004181.

Breshears, D. D., O. B. Myers, C. W. Meyer, F. J. Barnes, C. B. Zou, C. D. Allen, N. G. McDowell, and W. T. Pockman (2009), Tree die-off in response to global change-type drought: Mortality insights from a decade of plant water potential measurements, *Front. Ecol. Environ.*, *7*(4), 185–189.

Brodribb, T. J., and H. Cochard (2009), Hydraulic failure defines the recovery and point of death in water-stressed conifers, *Plant Physiol.*, *149*(1), 575–584.

Brodribb, T. J., and N. M. Holbrook (2006), Declining hydraulic efficiency as transpiring leaves desiccate: Two types of response, *Plant Cell Environ.*, *29*(12), 2205–2215.

Brodribb, T. J., and S. A. M. McAdam (2013), Abscisic acid mediates a divergence in the drought response of two conifers, *Plant Physiol.*, *162*(3), 1370–1377.

Brodribb, T., N. Holbrook, and M. Gutierrez (2002), Hydraulic and photosynthetic co-ordination in seasonally dry tropical forest trees, *Plant Cell Environ.*, *25*(11), 1435–1444.

Bucci, S. J., G. Goldstein, F. C. Meinzer, A. C. Franco, P. Campanello, and F. G. Scholz (2005), Mechanisms contributing to seasonal homeostasis of minimum leaf water potential and predawn disequilibrium between soil and plant water potential in Neotropical savanna trees, *Trees*, *19*(3), 296–304.

Campbell, G. S. (1985), *Soil Physics with Basic: Transport Models for Soil-Plant Systems*, Elsevier Sci., Amsterdam, Netherlands.

Campbell, G. S., and J. M. Norman (1998), *An Introduction to Environmental Biophysics*, Springer, N. Y.

Cochard, H., and S. Delzon (2013), Hydraulic failure and repair are not routine in trees, *Ann. Forest Sci.*, *70*(7), 659–661.

Comstock, J. P. (2002), Hydraulic and chemical signalling in the control of stomatal conductance and transpiration, *J. Exp. Bot.*, *53*(367), 195–200.

Da Silva, D., R. Favreau, I. Auzmendi, and T. M. DeJong (2011), Linking water stress effects on carbon partitioning by introducing a xylem circuit into L-PEACH, *Ann. Bot.*, *108*(6), 1135–1145.

dePury, D. G. G., and G. D. Farquhar (1997), Simple scaling of photosynthesis from leaves to canopies without the errors of big-leaf models, *Plant Cell Environ.*, *20*(5), 537–557.

Dickman, L. T., N. G. Mcdowell, S. Sevanto, R. E. Pangle, and W. T. Pockman (2014), Carbohydrate dynamics and mortality in a piñon-juniper woodland under three future precipitation scenarios, *Plant Cell Environ.*, *38*(4), 729–739.

Domec, J.-C., B. Lachenbruch, F. C. Meinzer, D. R. Woodruff, J. M. Warren, and K. A. McCulloh (2008), Maximum height in a conifer is associated with conflicting requirements for xylem design, *Proc. Natl. Acad. Sci. U. S. A.*, *105*(33), 12,069–12,074.
Domec, J. C., J. Ogée, A. Noormets, J. Jouangy, M. Gavazzi, E. Treasure, G. Sun, S. G. McNulty, and J. S. King (2012), Interactive effects of nocturnal transpiration and climate change on the root hydraulic redistribution and carbon and water budgets of southern United States pine plantations, *Tree Physiol.*, *32*(6), 707–723.
Ewers, B., R. Oren, and J. Sperry (2000), Influence of nutrient versus water supply on hydraulic architecture and water balance in Pinus taeda, *Plant Cell Environ.*, *23*(10), 1055–1066.
Ewers, B. E., D. S. Mackay, and S. Samanta (2007), Interannual consistency in canopy stomatal conductance control of leaf water potential across seven tree species, *Tree Physiol.*, *27*(1), 11–24.
Farquhar, G. D., and T. D. Sharkey (1982), Stomatal conductance and photosynthesis, *Annu. Rev. Plant Physiol. Plant Mol. Biol.*, *33*, 317–345.
Farquhar, G. D., S. V. Caemmerer, and J. A. Berry (1980), A biochemical-model of photosynthetic Co2 assimilation in leaves of C-3 species, *Planta*, *149*(1), 78–90.
Fisher, J. B., R. J. Whittaker, and Y. Malhi (2011), ET come home: Potential evapotranspiration in geographical ecology, *Global Ecol. Biogeogr.*, *20*(1), 1–18.
Franklin, O., J. Johansson, R. C. Dewar, U. Dieckmann, R. E. McMurtrie, A. Brannstrom, and R. Dybzinski (2012), Modeling carbon allocation in trees: A search for principles, *Tree Physiol.*, *32*(6), 648–666.
Franks, P. J. (2004), Stomatal control and hydraulic conductance, with special reference to tall trees, *Tree Physiol.*, *24*(8), 865–878.
Franks, P. J., P. L. Drake, and R. H. Froend (2007), Anisohydric but isohydrodynamic: Seasonally constant plant water potential gradient explained by a stomatal control mechanism incorporating variable plant hydraulic conductance, *Plant Cell Environ.*, *30*(1), 19–30.
Gaylord, M. L., T. E. Kolb, W. T. Pockman, J. A. Plaut, E. A. Yepez, A. K. Macalady, R. E. Pangle, and N. G. Mcdowell (2013), Drought predisposes piñon-juniper woodlands to insect attacks and mortality, *New Phytol.*, *198*(2), 567–578.
Gholz, H. (1982), Environmental limits on aboveground net primary production, leaf area, and biomass in vegetation zones of the Pacific Northwest, *Ecology*, 469–481.
Grier, C., and S. Running (1977), Leaf area of mature northwestern coniferous forests: relation to site water balance, *Ecology*, *58*(4), 893–899.
Gustafson, E. J., A. M. G. De Bruijn, R. E. Pangle, J. M. Limousin, N. G. Mcdowell, W. T. Pockman, B. R. Sturtevant, J. D. Muss, and M. E. Kubiske (2014), Integrating ecophysiology and forest landscape models to improve projections of drought effects under climate change, *Global Change Biol.*, *21*(2), 843–856.
Hacke, U. G., V. Stiller, J. S. Sperry, J. Pittermann, and K. A. McCulloh (2001), Cavitation fatigue. Embolism and refilling cycles can weaken the cavitation resistance of xylem, *Plant Physol.*, *125*(2), 779–786.
Hacke, U. G., J. S. Sperry, B. E. Ewers, D. S. Ellsworth, K. V. R. Schafer, and R. Oren (2000), Influence of soil porosity on water use in Pinus taeda, *Oecologia*, *124*(4), 495–505.
Hickler, T., I. C. Prentice, B. Smith, M. T. Sykes, and S. Zaehle (2006), Implementing plant hydraulic architecture within the LPJ Dynamic Global Vegetation Model, *Global Ecol. Biogeogr.*, *15*, 567–577.
Holtta, T., M. Mencuccini, and E. Nikinmaa (2009), Linking phloem function to structure: Analysis with a coupled xylem-phloem transport model, *J. Theor. Biol.*, *259*(2), 325–337.
Holtta, T., T. Vesala, S. Sevanto, M. Peramaki, and E. Nikinmaa (2006), Modeling xylem and phloem water flows in trees according to cohesion theory and Munch hypothesis, *Trees Struct. Funct.*, *20*(1), 67–78.
Hubbard, R. M., B. J. Bond, and M. G. Ryan (1999), Evidence that hydraulic conductance limits photosynthesis in old Pinus ponderosa trees, *Tree Physiol.*, *19*(3), 165–172.
Hultine, K. R., D. F. Koepke, W. T. Pockman, A. Fravolini, J. S. Sperry, and D. G. Williams (2006), Influence of soil texture on hydraulic properties and water relations of a dominant warm-desert phreatophyte, *Tree Physiol.*, *26*(3), 313–323.
Janott, M., S. Gayler, A. Gessler, M. Javaux, C. Klier, and E. Priesack (2010), A one-dimensional model of water flow in soil-plant systems based on plant architecture, *Plant Soil*, *341*(1–2), 233–256.
Johnson, N. C., C. Angelard, I. R. Sanders, and E. T. Kiers (2013), Predicting community and ecosystem outcomes of mycorrhizal responses to global change, *Ecol. Lett.*, *16*, 140–153.
Katul, G., R. Leuning, and R. Oren (2003), Relationship between plant hydraulic and biochemical properties derived from a steady-state coupled water and carbon transport model, *Plant Cell Environ.*, *26*(3), 339–350.
Katul, G. G., S. Palmroth, and R. Oren (2009), Leaf stomatal responses to vapour pressure deficit under current and CO 2-enriched atmosphere explained by the economics of gas exchange, *Plant Cell Environ.*, *32*(8), 968–979.
Klein, T. (2014), The variability of stomatal sensitivity to leaf water potential across tree species indicates a continuum between isohydric and anisohydric behaviours, *Funct. Ecol.*, *28*(6), 1313–1320.
Kolb, K. J., and J. S. Sperry (1999), Differences in drought adaptation between subspecies of sagebrush (Artemisia tridentata), *Ecology*, *80*(7), 2373–2384.
Larcher, W. (2003), *Physiological Plant Ecology: Ecophysiology and Stress Physiology of Functional Groups*, 4th ed., 513 pp., Springer, Berlin.
Limousin, J. M., S. Rambal, J. M. Ourcival, A. Rocheteau, R. Joffre, and R. Rodriguez-Cortina (2009), Long-term transpiration change with rainfall decline in a Mediterranean Quercus ilexforest, *Global Change Biol.*, *15*(9), 2163–2175.
Limousin, J. M., C. P. Bickford, L. T. Dickman, R. E. Pangle, P. J. Hudson, A. L. Boutz, N. Gehres, J. L. Osuna, W. T. Pockman, and N. G. Mcdowell (2013), Regulation and acclimation of leaf gas exchange in a piñon-juniper woodland exposed to three different precipitation regimes, *Plant Cell Environ.*, *36*(10), 1812–1825.
Linton, M. J., J. S. Sperry, and D. G. Williams (1998), Limits to water transport in Juniperus osteosperma and Pinus edulis: Implications for drought tolerance and regulation of transpiration, *Funct. Ecol.*, *12*(6), 906–911.
Loranty, M. M., D. S. Mackay, B. E. Ewers, E. Traver, and E. L. Kruger (2010a), Competition for light between individual trees lowers reference canopy stomatal conductance: Results from a model, *J. Geophys. Res.*, *115*, G04019, doi:10.1029/2010JG001377.
Loranty, M. M., D. S. Mackay, B. E. Ewers, E. Traver, and E. L. Kruger (2010b), Contribution of competition for light to within-species variability in stomatal conductance, *Water Resour. Res.*, *46*, W05516, doi:10.1029/2009wr008125.
Mackay, D. S., B. E. Ewers, M. M. Loranty, E. L. Kruger, and S. Samanta (2012), Bayesian analysis of canopy transpiration models: A test of posterior parameter means against measurements, *J. Hydrol.*, *432–433*, 75–83.
Magnani, F., J. Grace, and M. Borghetti (2002), Adjustment of tree structure in response to the environment under hydraulic constraints, *Funct. Ecol.*, *16*(3), 385–393.
Manzoni, S., G. Vico, G. Katul, S. Palmroth, and A. Porporato (2014), Optimal plant water-use strategies under stochastic rainfall, *Water Resour. Res.*, *50*, doi:10.1002/2014WR015375.

Maseda, P. H., and R. J. Fernandez (2006), Stay wet or else: Three ways in which plants can adjust hydraulically to their environment, *J. Exp. Bot.*, *57*(15), 3963–3977.
McAdam, S. A. M., and T. J. Brodribb (2014), Separating active and passive influences on stomatal control of transpiration, *Plant Physiol.*, *164*(4), 1578–1586.
McCulloh, K. A., and J. S. Sperry (2005), Patterns in hydraulic architecture and their implications for transport efficiency, *Tree Physiol.*, *25*(3), 257–267.
McDowell, N., et al. (2008), Mechanisms of plant survival and mortality during drought: Why do some plants survive while others succumb to drought?, *New Phytol.*, *178*(4), 719–739.
McDowell, N. G. (2011), Mechanisms linking drought, hydraulics, carbon metabolism, and vegetation mortality, *Plant Physiol.*, *155*(3), 1051–1059.
McDowell, N. G., D. J. Beerling, D. D. Breshears, R. A. Fisher, K. F. Raffa, and M. Stitt (2011), The interdependence of mechanisms underlying climate-driven vegetation mortality, *Trends Ecol. Evol.*, *26*(10), 523–532.
McDowell, N. G., et al. (2013), Evaluating theories of drought-induced vegetation mortality using a multimodel-experiment framework, *New Phytol.*, *200*(2), 304–321.
Meinzer, F. C., D. M. Johnson, B. Lachenbruch, K. A. Mcculloh, and D. R. Woodruff (2009), Xylem hydraulic safety margins in woody plants: Coordination of stomatal control of xylem tension with hydraulic capacitance, *Funct. Ecol.*, *23*(5), 922–930.
Mitchell, P. J., A. P. O'Grady, D. T. Tissue, D. A. White, M. L. Ottenschlaeger, and E. A. Pinkard (2013), Drought response strategies define the relative contributions of hydraulic dysfunction and carbohydrate depletion during tree mortality, *New Phytol.*, *197*(3), 862–872.
Monteith, J. L. (1965), Evaporation and environment, paper presented at 19th Symposium of the Society for Experimental Biology: The State amd Movement of Water in Living Organisms, Cambridge Univ. Press, Cambridge, U. K.
Nolf, M., K. Pagitz, and S. Mayr (2013), Physiological acclimation to drought stress in Solidago canadensis, *Physiol. Plant.*, *150*(4), 529–539.
Novick, K., R. Oren, P. Stoy, J. Y. Juang, M. Siqueira, and G. Katul (2009), The relationship between reference canopy conductance and simplified hydraulic architecture, *Adv. Water Resour.*, *32*(6), 809–819.
Oren, R., J. S. Sperry, G. G. Katul, D. E. Pataki, B. E. Ewers, N. Phillips, and K. V. R. Schafer (1999), Survey and synthesis of intra- and interspecific variation in stomatal sensitivity to vapour pressure deficit, *Plant Cell Environ.*, *22*(12), 1515–1526.
Plaut, J. A., E. A. Yepez, J. HILL, R. Pangle, J. S. Sperry, W. T. Pockman, and N. G. Mcdowell (2012), Hydraulic limits preceding mortality in a piñon-juniper woodland under experimental drought, *Plant Cell Environ.*, *35*(9), 1601–1617.
Plaut, J. A., W. D. Wadsworth, R. Pangle, E. A. Yepez, N. G. Mcdowell, and W. T. Pockman (2013), Reduced transpiration response to precipitation pulses precedes mortality in a piñon-juniper woodland subject to prolonged drought, *New Phytol.*, *200*(2), 375–387.
Pockman, W., and N. McDowell (2014a), *Ecosystem-Scale Rainfall Manipulation in a Piñon-Juniper Forest at the Sevilleta National Wildlife Refuge, New Mexico: Soil Temperature Data (2006-)*, Long-Term Ecol. Res. Network, Albuquerque, N. M. [Available at http://dx.doi.org/10.6073/pasta/1956560d489ca80ea7a95711cf73d67a.]
Pockman, W., and N. McDowell (2014b), *Ecosystem-Scale Rainfall Manipulation in a Piñon-Juniper Forest at the Sevilleta National Wildlife Refuge, New Mexico: Meteorological Data (2006-)*, Long-Term Ecol. Res. Network, Albuquerque, N. M. [Available at http://dx.doi.org/10.6073/pasta/a053a821b84c51356730b4ee05a10e3f.]
Pockman, W., and N. McDowell (2014c), *Ecosystem-Scale Rainfall Manipulation in a Piñon-Juniper Forest at the Sevilleta National Wildlife Refuge, New Mexico: Water Potential Data (2006-)*, Long-Term Ecol. Res. Network, Albuquerque, N. M. [Available at http://dx.doi.org/10.6073/pasta/40bb068de7083676cad39c8b7b51d122.]
Pockman, W. T., J. S. Sperry, and J. W. Leary (1995), Sustained and significant negative water pressure in xylem, *Nature*, *378*(6558), 715–716.
Press, W. H., S. A. Teukolsky, W. T. Vetterling, and B. P. Flannery (1992), *Numerical Recipes in C: The Art of Scientific Computing*, 2nd ed., Cambridge Univ. Press, Cambridge, England.
Quijano, J. C., P. Kumar, D. T. Drewry, A. Goldstein, and L. Misson (2012), Competitive and mutualistic dependencies in multispecies vegetation dynamics enabled by hydraulic redistribution, *Water Resour. Res.*, *48*, W05518, doi:10.1029/02011WR011416.
Ross, P. J., and K. L. Bristow (1990), Simulating water movement in layered and gradational soils using the Kirchhoff transform, *Soil Sci. Soc. Am. J.*, *54*(6), 1519–1524.
Running, S. W., and S. T. Gower (1991), FOREST-BGC, a general-model of forest ecosystem processes for regional applications: 2. Dynamic carbon allocation and nitrogen budgets, *Tree Physiol.*, *9*(1-2), 147–160.
Sala, A., and G. Hoch (2009), Height-related growth declines in ponderosa pine are not due to carbon limitation, *Plant Cell Environ.*, *32*(1), 22–30.
Sala, A., F. Piper, and G. Hoch (2010), Physiological mechanisms of drought-induced tree mortality are far from being resolved, *New Phytol.*, *186*(2), 274–281.
Samanta, S., D. S. Mackay, M. K. Clayton, E. L. Kruger, and B. E. Ewers (2007), Bayesian analysis for uncertainty estimation of a canopy transpiration model, *Water Resour. Res.*, *43*, W10701, doi:10.1029/2007wr006504.
Schafer, K., R. Oren, and J. Tenhunen (2000), The effect of tree height on crown level stomatal conductance, *Plant Cell Environ.*, *23*(4), 365–375.
Schlaepfer, D. R., B. E. Ewers, B. N. Shuman, D. G. Williams, J. M. Frank, W. J. Massman, and W. K. Lauenroth (2014), Terrestrial water fluxes dominated by transpiration: Comment, *Ecosphere*, *5*(5), 61.
Sevanto, S., N. G. Mcdowell, L. T. Dickman, R. Pangle, and W. T. Pockman (2013), How do trees die? A test of the hydraulic failure and carbon starvation hypotheses, *Plant Cell Environ.*, *37*(1), 153–161.
Singsaas, E. L., D. R. Ort, and E. H. DeLucia (2001), Variation in measured values of photosynthetic quantum yield in ecophysiological studies, *Oecologia*, *128*(1), 15–23.
Sperry, J., and U. Hacke (2002), Desert shrub water relations with respect to soil characteristics and plant functional type, *Funct. Ecol.*, *16*(3), 367–378.
Sperry, J. S., and D. M. Love (2015), Tansley review: What plant hydraulics can tell us about plant responses to climate-change droughts, *New Phytol.*, *207*, 14–27.
Sperry, J. S., F. R. Adler, G. S. Campbell, and J. P. Comstock (1998), Limitation of plant water use by rhizosphere and xylem conductance: Results from a model, *Plant Cell Environ.*, *21*(4), 347–359.
Tardieu, F., and W. J. Davies (1993), Integration of hydraulic and chemical signaling in the control of stomatal conductance and water status of droughted plants, *Plant Cell Environ.*, *16*(4), 341–349.
Tardieu, F., and T. Simonneau (1998), Variability among species of stomatal control under fluctuating soil water status and evaporative demand: Modelling isohydric and anisohydric behaviours, *J. Exp. Bot.*, *49*(special issue), 419–432.
Tuzet, A., A. Perrier, and R. Leuning (2003), A coupled model of stomatal conductance, photosynthesis and transpiration, *Plant Cell Environ.*, *26*(7), 1097–1116.

Tyree, M. T., and J. S. Sperry (1988), Do woody-plants operate near the point of catastrophic xylem dysfunction caused by dynamic water-stress: Answers from a model, *Plant Physiol.*, *88*(3), 574–580.
Tyree, M. T., and J. S. Sperry (1989), Vulnerability of xylem to cavitation and embolism, *Annu. Rev. Plant Biol.*, *40*(1), 19–36.
Van Genuchten, M. T. (1980), A closed-form equation for predicting the hydraulic conductivity of unsaturated soils, *Soil Sci. Soc. Am. J.*, *44*(5), 892–898.
Waring, R. H., and W. H. Schlesinger (1985), *Forest Ecosystems Concepts and Management*, 340 pp., Academic, San Diego, Calif.
West, A. G., K. R. Hultine, T. L. Jackson, and J. R. Ehleringer (2007), Differential summer water use by Pinus edulis and Juniperus osteosperma reflects contrasting hydraulic characteristics, *Tree Physiol.*, *27*(12), 1711–1720.
Whitehead, D., and P. G. Jarvis (1981), Coniferous trees and plantations, in *Water Deficits and Plant Growth*, edited by T. T. Kozlowski, pp. 49–152, Academic, N. Y.
Williams, M., E. Rastetter, D. Fernandes, M. Goulden, S. Wofsy, G. Shaver, J. Melillo, J. Munger, S. Fan, and K. Nadelhoffer (1996), Modelling the soil-plant-atmosphere continuum in a Quercus-Acer stand at Harvard Forest: The regulation of stomatal conductance by light, nitrogen and soil/plant hydraulic properties, *Plant Cell Environ.*, *19*(8), 911–927.
Williams, M., B. E. Law, P. M. Anthoni, and M. H. Unsworth (2001), Use of a simulation model and ecosystem flux data to examine carbon-water interactions in ponderosa pine, *Tree Physiol.*, *21*(5), 287–298.
Wilson, K. B., D. D. Baldocchi, and P. J. Hanson (2000), Spatial and seasonal variability of photosynthetic parameters and their relationship to leaf nitrogen in a deciduous forest, *Tree Physiol.*, *20*(9), 565–578.
Zwieniecki, M. A., and N. M. Holbrook (2009), Confronting Maxwell's demon: Biophysics of xylem embolism repair, *Trends Plant Sci.*, *14*(10), 530–534.